Non-marine carbon-isotope stratigraphy of the Triassic-Jurassic transition in the Polish Basin and its relationships to organic carbon preservation, pCO2 and palaeotemperature

Grzegorz Pieńkowski, Stephen P. Hesselbo, Maria Barbacka, Melanie J. Leng

PII: S0012-8252(20)30429-3

DOI: https://doi.org/10.1016/j.earscirev.2020.103383

Reference: EARTH 103383

To appear in: *Earth-Science Reviews*

Received date: 27 February 2020

Revised date: 27 August 2020

Accepted date: 24 September 2020

Please cite this article as: G. Pieńkowski, S.P. Hesselbo, M. Barbacka, et al., Non-marine carbon-isotope stratigraphy of the Triassic-Jurassic transition in the Polish Basin and its relationships to organic carbon preservation, pCO2 and palaeotemperature, *Earth-Science Reviews* (2020), https://doi.org/10.1016/j.earscirev.2020.103383

Non-marine carbon-isotope stratigraphy of the Triassic-Jurassic transition in the Polish Basin and its relationships to organic carbon preservation, pCO_2 and palaeotemperature

[1]Grzegorz Pieńkowski, [2]Stephen P. Hesselbo, [3]Maria Barbacka, [4]Melanie J. Leng

[1]Polish Geological Institute – National Research Institute, Rakowiecka 4, PL-00-975 Warszawa, Poland; grzegorz.pienkowski@pgi.gov.pl (corresponding author)

[2]Camborne School of Mines and Environment and Sustainability Institute, University of Exeter, Penryn TR10 9FE, UK; s.p.hesselbo@exeter.ac.uk

[3]W. Szafer Institute of Botany, PAN, ul. Lubicz 46, PL- 31-512 Kraków, Poland; Department of Botany, Hungarian Natural History Museum, H-1476 Budapest, P.O. Box 222, Hungary; maria.barbacka@gmail.com.

[4]National Environmental Isotope Facility, British Geological Survey, Nottingham NG12 5FF, UK and Centre for Environmental Geochemistry, School of Biosciences, University of Nottingham, LE12 5RD, UK; mjl@bgs.ac.uk

Abstract

New carbon-isotope data obtained from homogenous organic material (separated microfossil wood; $\delta^{13}C_{wood}$) from the upper Rhaetian and entire Lower Jurassic permit chemostratigraphic correlation of these marginal/non-marine deposits with the biostratigraphically well-constrained Llanbedr (Mochras Farm) core in N Wales and other marine profiles, supported by sequence stratigraphic correlation and biostratigraphical markers. Statistically significant (Rs = 0.61) positive exponential correlation between $\delta^{13}C_{wood}$ values and continental TOC (TOC_{cont}) concentrations occurs and can be defined empirically by equation. Changes of $\delta^{13}C_{wood}$ observed in C3 plants depends on $\delta^{13}CO_2$ of atmosphere and can be modulated by other factors such as pCO_2 causing fractionation (enrichment in ^{12}C) of C isotopes in source C3 plants and, to lesser extent, by soil moisture content. Floral remains occurring in the relatively stable palaeolatitude and climatic zone of the Polish Basin in the time interval studied lend no support for significant precipitation impact on the $\delta^{13}C$ fractionation, although enhanced precipitation could have had a limited impact during the Toarcian Oceanic Anoxic Event (T-OAE). We argue that the observed relation between $\delta^{13}C_{wood}$ values and TOC_{cont} reflects the global carbon cycle forcing. Such correlations may develop because fluxes of of ^{12}C-enriched methane, mobilized from near-surface carbon sources, lead to global warming, decreased $\delta^{13}C_{wood}$ and enhanced (usually fungally-mediated) decomposition of the terrestrial carbon pool, while subsequent massive burial of organic carbon results in higher $\delta^{13}C$ values in all carbon cycle reservoirs, and the attendant drawdown of atmospheric CO_2 leads to global cooling and promotes sequestration of soil organic matter. In turn, this relation can be used as an indirect indicator of atmospheric temperature trends, although organic carbon isotope records are potentially subject to many different influences. Based on the $\delta^{13}C_{wood}$ /TOC_{cont} relationship, an approximate qualitative estimation of general trends in air temperature is suggested for c. 40°N paleolatitude and the warm temperate climatic zone. The observed hypothetical trends in temperature are generally in

concordance with pCO_2 trends calculated from stomatal index. A weak $\delta^{13}C_{wood}$ and TOC_{cont} correlation in Rhaetian deposits is explained by local environmental factors (TOC concentration dependent on a more localized fluvial plain settings), while mostly deltaic – coastal deposits contain more representative, averaged material delivered from a large catchment area.

Key words: Chemostratigraphy, correlation, paralic facies, palaeoclimate, carbon isotopes

1. Introduction

Correlation of biostratigraphically-constrained marine sections with marginal-marine or continental deposits with poor biostratigraphical control is regarded as one of most complex and challenging, yet very important, problems in stratigraphy. As shown for example by Hesselbo and Pieńkowski (2011), carbon-isotope ($\delta^{13}C$) chemostratigraphy provides a means of age correlation for strata deposited in diverse marine and non-marine depositional environments. However, such correlations are reliable only when appropriate profiles are accessible. In particular, long, cored borehole sections offer the opportunity to reconstruct Earth system evolution in the geological past and contain, for example, the records of tectonic, carbon cycle, climatic and biological cycles. Expanded core sections, providing a continuous record of the Lower Jurassic series – such as the Llanbedr (Mochras Farm) core recovered in Wales, UK (Woodland, 1971; Katz et al, 2005; Hesselbo et al, 2013; Ruhl et al, 2016; Xu et al, 2018; Storm et al, 2020), hereafter referred to as Mochras, and Kaszewy borehole drilled in central Poland (Figs. 1, 2), are exceptionally valuable. The isotope ratios of atmospheric CO_2 ($\delta^{13}CO_2$) to a certain degree reflect perturbations in atmospheric C fluxes (e.g. Pagani et al 2006 for the PETM case), and therefore estimates of $\delta^{13}CO_2$ are central to estimating past climate sensitivity to changes in atmospheric CO_2 pressure (pCO_2). While inputs of isotopically light carbon to the atmosphere-ocean system result in decreasing $\delta^{13}CO_2$ and increasing pCO_2 recorded as a negative carbon isotope excursion in both inorganic and organic carbon enhanced burial of organic carbon and enhanced silicate weathering leads to a fall in atmospheric pCO_2, and a positive excursion (Gröcke et al 1999; Kump and Arthur 1999). The pCO_2 and related temperature is a basic climate variable, yet its estimates in deep geological past are difficult and often controversial as the carbon cycle involves multiple sources and sinks in a dynamic rather than a static mass-balance equilibrium (Kump and Arthur 1999). The near surface carbon cycling, such as release of methane clathrates, permafrost destruction, decomposition of soil organic matter (acting as a source of ^{13}C-depleted carbon) and burial of organic matter and carbonate or silicate weathering (acting as a sink – Cohen et al 2004; Them et al 2017b; Kump 2018; Ullmann et al 2020) played a major role in modulating atmospheric carbon concentrations. Nevertheless, values of $\delta^{13}C_{TOC}$ which come from

sedimentary rocks (specifically, the values obtained from fossil plants) are widely used to estimate $\delta^{13}C$ of ancient plants and infer changes in $\delta^{13}CO_2$. Additionally, $\delta^{13}C$ depends on pCO_2 - the higher pCO_2, the stronger fractionation of $\delta^{13}C$ by plants towards light values. Thus the currently debated effect of CO_2 concentration on $^{13}C/^{12}C$ ratios ($\delta^{13}C$) is crucial to reconstructing ancient environments and quantifying the carbon cycle (Hare et al 2018; Ruebsam et al 2020).

Currently most of the temperature estimates for this time interval have been based principally on oxygen isotopes ($\delta^{18}O$) from calcareous macrofossils, such as oysters, brachiopods and belemnites, or calcareous nannofossils (Suan et al 2008, 2010; Korte and Hesselbo 2011; Dera et al 2011; Silva and Duarte 2015; Gómez et al 2016; Price et al, 2016; Peti and Thibault, 2017 – for recent comprehensive summary see Ruebsam et al 2020) from European marine sections. However, temperature interpretation based on $\delta^{18}O$ can be distorted by changes in the local source(s) of water and local/regional evaporation-precipitation dynamics as well as diagenesis, and therefore choosing the sites and samples unaffected by these processes is essential. Furthermore, the thermal perturbations are likely to have been controlled also by the silicate weathering flux, in the case of the Lower Jurassic extending these times of warmth by limitation of the global silicate weathering flux (e.g. Ullmann et al 2020). It should be noted that Os-isotope proxies from eastern and western Panthalassa show a modest decline in weathering intensity after the peak of the negative carbon-isotope excursion of the T-OAE (Them et al 2017b, Kemp et al 2020. Nevertheless, a broadly synchronous coupling between massive carbon release and enhanced global continental crust weathering during T-OAE is not controversial. Estimating palaeotemperatures based on $\delta^{18}O$ is also prone to problems such as the vital effects of the organism precipitating the carbonate (Price 2017). Herein, we discuss $\delta^{13}C_{wood}$ values and their relation to TOC_{cont} in context of the global carbon cycle and resulting interpretation of climate changes - including temperature trends – with particular reference to the Kaszewy core.

2. Geological setting

The Polish Basin is a large, now tectonically inverted, sedimentary basin covering most of modern-day Poland, and representing the eastern arm of the NE European epicontinental basin (Dadlez et al 1998; Dadlez, 2003) – Fig. 1. The upper Rhaetian strata and the whole Lower Jurassic series belong to the Kamienna Group composed of siliciclastic deposits (mudstones, sandstones) with subordinate conglomerate, coaly and siderite beds. Throughout the Mesozoic, regional subsidence patterns in the Polish Basin were dominated by the development of the NW–SE-trending Mid-Polish Trough, which was filled with up to 8000 m of Permian–Mesozoic sediments, of which c. 1200-1300 m belongs to the Kamienna Group (Pieńkowski, 2004). Intermittently, this long-term thermal subsidence was influenced by local modifications imposed mainly by lateral salt movements in its central and NW segments, creating salt pillows. The Kaszewy borehole is situated at a slope of one of these broad

and flat pillows, called Wojszyce structure (Dadlez 1998). In the latest Triassic – Early Jurassic times the Polish basin was located at a latitude about 40°N, within a warm temperate/winter-wet climate belt (e.g. Rees et al 2000; Dera et al, 2009). Sedimentology, lithofacies, ichnofacies, biofacies as well as sequence stratigraphy and palaeogeography of the NE European basin have been studied for decades and published in number of papers (Dadlez and Kopik 1972; Pieńkowski 2004, 2014, 2015; Pieńkowski, Schudack et al., 2008; Pieńkowski & Waksmundzka, 2009; Hesselbo & Pieńkowski, 2011; Pieńkowski et al, 2012, 2014, 2016; Barth et al., 2018 a, b).

The latest Rhaetian and Early Jurassic were times of extreme environmental change. Through this period there are well-documented examples of enhanced volcanic activity, rapid transitions from cold, or even glacial climates, through to super-greenhouse events, multiple large-magnitude isotopic anomalies, global sea-level changes, and mass extinctions. These events not only reflect changes in the global climate system but are also thought to have had significant influence on the evolution of Jurassic marine and terrestrial biota. However, our knowledge to date is fragmentary, largely because of the fragmentary and discontinuous nature of the existing datasets – particularly, with respect to atmospheric/terrestrial realm. Studies hitherto have largely focused on two events, connected to the development of Large Igneous Provinces (LIPs): Central Atlantic Magmatic Province (CAMP) at the Rhaetian-Hettangian transition, and early Toarcian Karoo-Ferrar Large Igneous Province, connected with the Toarcian Oceanic Anoxic Event (T-OAE – Jenkyns, 1988). While marine strata have been studied more extensively in terms of oceanographic, climatic and biological processes (Korte and Hesselbo 2011, Dera et al 2011; Lindström et al 2012, 2017; Harazim et al 2013; Suan et al 2015; Ruhl et al 2016; Them et al 2018; Van de Schootbrugge et al 2019; Storm et al 2020), reports from continental or marginal-marine materials remain relatively sparse (e.g. Pieńkowski 2004, 2014; McElwain et al 2005; Hesselbo and Pieńkowski 2011; Pieńkowski et al 2012, 2014, 2016; Them et al 2017 a,b; Baker et al 2017; Xu et al 2017; Ruebsam et al 2019; Liu et al 2020). Records in epicontinental seaways may potentially show a pronounced regional overprint on carbon isotope composition of sedimentary organic matter (McArthur et al 2008; Ruhl et al 2010), usually resulting from mixing of different organic components (Suan et al 2015), but results obtained from homogenous woody material ($\delta^{13}C_{wood}$) are more reliable in interpreting global changes more directly, as they reflect atmospheric (i.e. global) processes (Gröcke 2002) and can therefore be used more confidently for chemostratigraphic correlations (see for Lower Jurassic examples: Hesselbo and Pieńkowski 2011; Pieńkowski et al 2016; Them et al 2017 b; Ruebsam et al 2020; Storm et al., 2020).

3. Materials and Methods

3.1. Lithology and stratigraphy

A new and unique geological archive (2050.6 m through the Norian - Rhaetian- Lower Jurassic strata) comes from the Kaszewy 1 borehole (Fig. 1), drilled in central Poland (52˚ 12′ 00.06″ N; 19˚ 29′ 35.38″ E) by PGE (*Polish Energy Group*) in order to characterize the potential for carbon capture and storage (CCS) in that area. The entire core has been thoroughly logged and sampled. Samples for geochemical analyses have been taken from similar lithologies (mudstones) in order to avoid lithological bias. The length and continuity of the Kaszewy core (98 % core recovery) is essential in studying continental or marginal-marine deposits by sedimentological methods and allowing application of isotope chemostratigraphy of these facies, supported by sequence stratigraphy and some biostratigraphical markers (Fig. 2). For comparison to Kaszewy we use the new compilation from the biostratigraphically constrained Mochras core (Storm et al, 2020) which covers the entire Early Jurassic, reproducing large-amplitude $\delta^{13}C_{TOC}$ excursions (>3 ‰) at the Sinemurian–Pliensbachian transition and in the lower Toarcian *serpentinum* Zone, as well as several previously identified medium-amplitude (~0.5–3 ‰) shifts in the Hettangian to Pliensbachian. In addition, $\delta^{13}C_{wood}$ (Storm et al, 2020) and $\delta^{13}C_{carb}$ (Katz et al 2005) data was also obtained (Fig. 2).

3.2. Carbon isotopes

Phytoclast samples for analysis were manually picked from HF palynomacerals and subsequently dried, weighed and sealed in tin capsules. Phytoclast samples were run at two laboratories, depending on their mass (Supplementary data 1). At the Research Laboratory for Archaeology and History of Art (RLAHA), University of Oxford, UK, larger samples were run on a Sercon Europa EA-GSL sample converter connected to a Sercon 20-22 stable isotope gas-ratio mass spectrometer running in continuous flow mode with a helium carrier gas with a flow rate of 70 ml per min. Carbon isotope ratios were measured against an internal alanine standard ($\delta^{13}C_{alanine}$ = –26.9 ± 0.2‰ V-PDB) using a single point calibration. The in-house RLAHA alanine standard is checked weekly against USGS40, USGS41 and IAEA-CH6 international reference materials. At the at the British Geological Survey, Nottingham, UK, smaller samples were analysed by combustion in a Costech Elemental Analyser (EA) on-line to a VG TripleTrap and Optima dual-inlet mass spectrometer, with $\delta^{13}C_{org}$ values reported relative to V-PDB following a within-run laboratory standard calibration, with NBS-18, NBS-19 and NBS-22. Replicate analysis of well-mixed samples show a reproducibility of ± <0.1‰ (1 SD).

3.3. Total Organic Carbon, Rock Eval 6 pyrolysis

Total Organic Carbon (TOC) analyses of 300 samples were performed using the chromatographic, coulometric method (procedure PB – 23) using an automated LECO analyser (Supplementary data 1). A total of 52 naturally carbonate-free mudstone samples (mostly those representing mixed environments – in order to evaluate which ones contain more marine kerogen) were analyzed in the

Rock Eval pyrolysis apparatus - model 6 Turbo (Vinci Technologies), in the laboratory of the Polish Geological Institute (Supplementary data 2). Crushed bulk rock material was thermally decomposed in a helium or nitrogen atmosphere. Every sample was heated to 650°C. The amount of free hydrocarbon (S1) thermally liberated from a rock sample at 300°C is measured using a Flame Ionization Detector (FID). Volatile components released during pyrolysis are separated into two streams. One of them passes through the FID and is registered as peak S2. Another volatile component released during pyrolysis, i.e., carbon dioxide generated from kerogen, is recorded by a thermal conductivity detector as the S3 peak. Repeat analyses of the parameters S1, S2, S3 and TOC agree within ±0.05. The Oxygen Index (OI, in mg CO2/g TOC) is calculated according to the formula (S3*100)/TOC. Hydrogen index (HI) = S2 (mg/g)/TOCx100. Only mudstone was sampled, therefore some parts of profile are sampled more sparsely due to the high sandstone content and sample spacing is heterogeneous. Coals and coaly mudstones were avoided as non-representative. Parts containing marine kerogen were sampled more sparsely. Only samples paired with $\delta^{13}C_{wood}$ data and of clearly continental origin (dominating kerogen type III and IV, about 80% of all samples) were used for δ^{13}_{wood}, TOC_{cont} and temperature interpretation (Fig. 2, Supplementary data 1, 2).

3.4. Stomatal index (SI)

Fifty-one specimens containing fossil plant remains from the Kaszewy core interval 1936.5-1296 m were studied. Only few levels contained well preserved remains with preserved cuticle, belonging mostly to genera *Baiera* Braun *emend* Florin and *Czekanowskia* Herr, on which the SI counting has been performed. Their determination was possible on a genus level only, but that is not a limitation for stomatal index study. *Baiera* and *Czekanowskia* are ginkgophytes, which means that all studied remains have the same nearest living equivalent species (NLEs), making ginkgophytes especially suitable for SI calculation (Beerling et al 1998; Xie et al 2006). The cuticles were prepared with standard methods in Schulze solution followed by 3% KOH. Only the surface of lower cuticle area within stomatal bands, was used for SI evaluation. The number of epidermal cells includes subsidiary cells. The investigated cuticle area was 300 × 300 µm = 0.09 mm^2 (the minimum area for SI calculation is 0.03 mm^2 - Jones and Rowe 1999). This area was adapted to the width of average stomatal band). SI was calculated according to Salisbury's equation: SI = [SD/(ED+SD)] ×100, where SI – stomatal index, SD – stomatal density (number of stomata/area), ED – number of epidermal cells/area (Jones and Rowe 1999). SI was counted according to Kürschner (1996), using 40 microphotographs for *Baiera* and 13 microphotographs for *Czekanowskia* (totally for 21 leaf fragments). For those specimens, 8-19 measurements were carried out, depending on the state of preservation. The atmospheric CO_2 level was estimated as 600 ppm × SR where SR is the Stomatal Ratio, i.e. SI of the nearest living equivalent divided by SI of fossil plant: SR = SI of NLEs/SI fossil.

Standardization was applied after Berner and Kathavala (2001) and SI for the extant *Ginkgo biloba* was used according to Beerling and Royer (2002a), as 9.1 at 350 ppm. Based on this relationship, palaeoatmospheric CO_2 pressure (pCO_2) was estimated, using stomatal parameters of fossil plants – stomatal density (SD) and stomatal index (SI) in relation with parameters of their NLEs, defined as the stomatal ratio (SR) (Beerling and Royer 2002a; Beerling and Royer 2002b; Royer et al 2001) . Plant reaction appears in leaf structure, especially in stomatal density, which is closely associated with fluctuations of atmospheric pCO_2 and displays an inverse correlation to pCO_2 (Woodward 1987; Beerling 1999; Pole and Kürschner 1999; Mosbrugger 1999; Royer et al 2001; Haworth and Raschi 2014). SI may be influenced by many factors that affect plants during their life, but, as has been discussed by many authors Chen et al 2001; Erdei et al 2012), the estimated pCO_2 values are not invalidated (except very young, undeveloped leaves which are not appropriate to SI calculation).

4. Results

4.1. Stratigraphy

The sediments studied yielded very few animal body fossils. Of note is a single find of ammonite *Tragophylloceras* cf. *loscombi* (Sowerby) in a 1.5 m thick grey shale at a depth of 1281.5 m (Pieńkowski 2015). The stratigraphical range of this species is rather wide, ranging from upper lower Pliensbachian to lower upper Pliensbachian (from the upper part of the *ibex* Zone/ *centaurus* Subzone to the upper part of the *subnodosus* Subzone of the *margaritatus* Zone (Howarth and Donovan 1964). Other methods, such as sequence stratigraphy (Pieńkowski 2004; Barth et al 2018) and carbon isotope chemostratigraphy point to the uppermost part of this ammonite's range, i.e. *subnodosus* Subzone. Next, some palynomorphs provide constraints on the Triassic – Jurassic boundary. Of note are common appearances of *Ricciisporites tuberculatus* Lundblad, a pollen assigned to an enigmatic gymnosperm and known for its common occurrences in the Rhaetian (Lindström et al 2017), with a last occurrence of 1890.2 m. Slightly above (1879 m) there is also the last occurrence of *Brachysaccus neomundanus* (Leschik) Madler, which was previously described from Rhaetian deposits in NW Poland (Pieńkowski et al 2012, 2014). Above a barren sandstone interval, new taxa appear: *Dictyophyllidites mortoni* (de Jersey) Playford & Dettmann at 1830.7 m - a spore common in the Hettangian assemblage in NW Poland (Pieńkowski et al 2012) and, more importantly, pollen grain *Cerebropollenites thiergartii* Schulz (1822.8 m), the only post-Triassic miospore with the first occurrence (FO) close to the base of the Jurassic (Hillebrandt et al 2013). These finds allow placement of the Triassic/Jurassic boundary between 1830.7 and 1879 m, likely at the secondary $\delta^{13}C_{wood}$ negative peak, correlatable with the similar peak in the St Audries Bay profile, southern UK (Korte et al. 2009).

For chemostratigraphic correlation of the Lower Jurassic succession, the best prospect lies in carbon isotope values obtained from similar material ($\delta^{13}C_{organic,}$ $\delta^{13}C_{wood}$) because, with the exception of purely pelagic carbonate palaeoenvironments, the carbon-isotope signature of any carbonate present is vulnerable to diagenesis, which is also borne out in the $\delta^{13}C_{carb}$ curve from Mochras presented by Katz et al (2005). However, comparison between the $\delta^{13}C_{org,}$ $\delta^{13}C_{wood}$ and $\delta^{13}C_{carb}$ curves can still be useful in indicating the most reliable primary CIEs; therefore selected $\delta^{13}C_{carb}$ curves can also be used, particularly if $\delta^{13}C_{org}$ curves are not available (Fig. 3). Chemostratigraphical correlation of Mochras and Kaszewy is uniquely valuable, as these two profiles are the most expanded, continuous cored sections of the Lower Jurassic series. Occurrences of some palynomorph taxa and the single ammonite in the Kaszewy borehole allowed positioning of the Triassic-Jurassic boundary and confirmed Pliensbachian or Toarcian age of the respective intervals. Overall, biostratigraphical constraints are of poor resolution. In addition, sequence stratigraphic correlation of depositional sequences and parasequences within the Polish basin and the Central European basin (Pieńkowski 2004; Barth et al 2018) provided an effective complementary stratigraphic framework for the Kaszewy profile. For the Rhaetian, the section at St Audrie's Bay (Hesselbo et al 2002; Ruhl et al 2010 is used for chemostratigraphic correlation with Kaszewy (Figs. 2, 3).

To interpret our Kaszewy $\delta^{13}C_{wood}$ curve, we compared it with Mochras and nine other published carbon isotope curves for the same time interval (Figs. 2, 3, 4). A continuous $\delta^{13}C_{wood}$ curve (Fig. 2) is constructed based on data obtained from homogenous terrestrial organic matter (phytoclast separates), thus reflecting isotope changes in atmospheric carbon cycle (Hesselbo and Pieńkowski 2011; Pieńkowski et al 2016; Them et al 2017 a), although other factors such as kinetic isotope fractionations should be also considered as additional factors. The general pattern of the curve shows more negative values (mostly below –27 ‰, with minimum of –28.3 ‰) in the strata assigned (based also on palynomorphs) to the Rhaetian (1905 – 1979 m) with three more prominent negative CIEs. Upwards from the Triassic/Jurassic boundary the $\delta^{13}C_{wood}$ values show a general, long-term trend towards heavier values, punctuated by five conspicuous negative CIEs (Figs. 1, 2). This trend is reversed at 1445.9 m and then again continuing upwards towards heavier values, with the heaviest value (–22.9 ‰) recorded in the upper Pliensbachian at 1266 m. A series of five prominent, step-wise CIEs (down to –30.6 ‰ at 1237.5 m, starting at 1247.3 m and ending at 1188.7 m) is assigned to the Toarcian Oceanic Anoxic Event/ T-OAE, called also Jenkyns Event) and can be clearly correlated with reference profiles of Mochras, Yorkshire, Peniche, and the composite reference profile by Ruebsam and Al-Husseini (2020) – Fig. 4. The major negative excursion of the T-OAE is unambiguous and has already been recognised in (with further biostratigraphic constraint) in many locations across the same basin (Hesselbo et al. 2000, Hesselbo and Pienkowski 2011). From 1188.7

m upwards the $\delta^{13}C_{wood}$ values stabilize at a level with a median c. –24 ‰. The section above the T-OAE is a special case because it has already been demonstrated that the lower Toarcian is commonly truncated in the Polish Basin beneath younger Toarcian strata (Pieńkowski 2004, Hesselbo and Pieńkowski 2011).

All conspicuous negative CIEs can be correlated with the $\delta^{13}C$ curves from the Mochras borehole (Katz et al 2005; Storm et al 2020) and from the St Audrie's Bay section for the Rhaetian (Korte et al, 2009; Ruhl et al 2010); Fig. 2). $\delta^{13}C_{wood}$ values from Kaszewy are averagely and systematically heavier by about 1‰ than the corresponding values from $\delta^{13}C_{TOC}$ values from Mochras, likely due to contributions from marine organic matter to the Mochras curve (Storm et al., 2020), but what is important for chemostratigraphic correlation is concordance in general trends. This average $\delta^{13}C$ contrast disappears considering the results of $\delta^{13}C_{wood}$ from Mochras. The correlation presented shows also a general concordance with other biostratigraphically constrained $\delta^{13}C$ curves from marine sections in Europe and North America, e.g. almost complete Lower Jurassic section from Schandelah in Germany (Van de Schootbrugge et al 2019), Rhaetian-Hettangian in Danish Basin (Lindström et al 2012) and North America (Whiteside et al 2010; Bartolini et al 2012), Sinemurian-Pliensbachian in Yorkshire, UK (Korte and Hesselbo 2011), Hettangian to Pliensbachian in Dorset, UK (Schöllhorn et al 2020) , Sinemurian-Pliensbachian in Spain (Gomez et al 2015), Sinemurian in the UK (Riding et al 2013; Hesselbo et al. 2020a), the Pliensbachian in the western US (De Lena et al. 2019), Pliensbachian and Toarcian in Portugal (Fantasia et al 2019) and France (Hermoso and Pellenard 2014) – Fig. 3, Supplementary data 3. In Mochras (Storm et al 2020) and Dorset (Schöllhorn et al 2020), there is a uncertainty with the placement of the upper Sinemurian CIE, labelled S2 in Figs 2, 3. In other reports, the conspicuous negative CIE occurs in the *oxynotum* zone, while in Mochras and Dorset the negative CIE occurs within the *obtusum* zone. The answer could be missing section (particularly in Dorset) or imprecise biostratigraphy. In the meantime, the stratigraphical position of this CIE in Mochras and Kaszewy remains open – it can be either of *obtusum* or *oxynotum* age. It should be noted, that some parts of the profile at Kaszewy represent reduced or condensed sections, particularly at the sequence boundaries (e.g. the Pliensbachian section). There are some reductions in thickness of Pliensbachian section observed between Kaszewy (located at the side of salt pillow) and Krośniewice borehole (located between salt structures 20 km to the NW – Dadlez 1973). Likely, these reductions can be attributed to salt movements and resulting hiatuses occurring at the sequence and parasequence boundaries. This could explain somewhat contrasting shapes of the Mochras ($\delta^{13}C_{TOC}$) and Kaszewy ($\delta^{13}C_{wood}$) carbon isotope curves in the uppermost Sinemurian-lower Pliensbachian interval. However, comparison of the $\delta^{13}C_{wood}$ curves is more compatible. Here we also provide an alternative correlation diagram for this interval, which

illustrates the more and the less likely scenario (Fig. 2). Nevertheless, correlation of this section is supported by sequence stratigraphy. The beginning of the Pliensbachian was connected with the major transgression in Polish basin, documented by ammonites in Pomerania and correlatable with NE European basins (Kopik and Dadlez 1972; Pieńkowski 2004; Barth et al. 2018). This widespread transgression is documented in Kaszewy by the appearance of marine kerogen and marine plankton (Pieńkowski 2015; Barth et al 2018). Concerning $\delta^{13}C$ correlations, sections of Yorkshire (Korte and Hesselbo 2011; Hesselbo et al. 2020a) and Dorset (Schöllhorn et al 2020) confirm the characteristic pattern of CIE excursions, with the lowermost Pliensbachian negative CIE preceded by a sharp positive CIE excursion in the uppermost Sinemurian. Such a pattern occurs also in Kaszewy between 1442 and 1450 m (Figs. 2, 3).

4.2. Total organic carbon (TOC), kerogen analyses

In the Rhaetian strata, TOC is usually below 1%, except for some darker mudstones interpreted to have been deposited in local ponds and lakes, where TOC content can reach 4% and more. The lowermost part of the Rhaetian strata is represented by red beds yielding very few or no palynomacerals (Supplementary data 1) and these strata are excluded from further considerations concerning TOC and $\delta^{13}C_{wood}$ as non-representative. In the Hettangian section TOC is in places abundant (Fig. 2), but most of these intervals contain marine kerogen (Supplementary data 2) occurring mostly in strata coeval with major transgressions of the *planorbis* and *liasicus* zones (Pieńkowski 2004; Barth et al 2018). In the upper Sinemurian – lower Pliensbachian section the studied samples usually contain more than 1% (1.14% in average). Moreover, a few beds have TOC up to 3-5 %, and the sample from the lowest part of Pliensbachian (depth of 1462.3 m) contains organic carbon as high as 15.3%. These samples contain marine kerogen associated with the *jamesoni-ibex* transgression and maximum flooding surface (Pieńkowski 2004; Barth et al 2018). In the upper Pliensbachian – Toarcian section TOC is usually in the range of 0 to 3% (1.0% on average). In contrast, most of the lower Toarcian is characterized by a low content of TOC (usually below 0.5%). In order to check the character of the kerogen, 52 mudstone samples from selected sections (based on sedimentological studies) were screened using RockEval 6 pyrolysis and interpreted using the Van Krevelen plot (Supplementary data 2). Kerogen was classified in classical types II, III and IV (type I has not been found), ranged in the order of H/C ratio obtained from the RockEval6 analyses. Type II originated in a shallow marine environment with phytoplanktonic input as the primary source. Type III and IV are found in deltaic/fluvial and coastal settings and derive from higher plant debris, commonly highly reworked and often degraded by fungi (Fig. 6). Type IV is considered as heavily altered Type III with very low H/C or Hydrogen Index and containing only the most resistant chemical

constituents of the terrestrial OM (inertinite). Type II is usually mixed with kerogen Type III. Samples containing only kerogen type III and IV (in total 224 samples) were taken for $\delta^{13}C_{wood}$ to TOC_{cont} interpretation (Figs. 2, 5; Supplementary data 1, 2).

4.3. Carbon isotope – total organic carbon ratio

The cross-plot of the $\delta^{13}C_{wood}$ to TOC_{cont} ratio (224 Rhaetian and Lower Jurassic samples: Fig. 5) shows significant positive correlation between the two variables with Pearson correlation coefficient r = 0.53 (R2=0.28) for linear fit and r=0.59 and R^2=0.59 for exponential fit. In both cases the p-value is <0.5. The result is statistically significant at p<.05. The Spearman's Rank Correlation Coefficient (Rs) has been also applied, as it is more appropriate in the case of exponential correlation: Rs = 0.61; p = 6.44^{-24} (for all 224 samples), the result is significant with the significance threshold 0.001 (Supplementary data 4). Samples are shown with symbols representing their stratigraphical position (Fig. 5). Rs = 0.61 for all samples containing continental kerogen is satisfactory for demonstrating a statistically significant trend/correlation, classified (depending on literature) as a moderate or strong (Evans 1996), while the Rhaetian section (66 samples) is characterized by a weak linear positive correlation of r = 0.16, with a noticeable number of outliers. The correlation coefficients are highest when applying exponential law fits, and slightly degrade when using linear fits (with exception of the Rhaetian, where linear fit is slightly higher).

4.4. Stomatal index and pCO_2

The SI and pCO_2 could be calculated only in six levels, but four of them occurred in the relatively narrow upper Hettangian interval, and as they suggest marked fluctuations of pCO_2, they could be compared with results obtained from the corresponding $\delta^{13}C_{wood}$ results. SI and pCO_2 values were calculated from ginkgophytes: *Czekanowskia* sp. 1 - upper Hettangian, 1694.2 m (1400 +/- 200 ppm CO_2); *Baiera* sp. 2 - upper Hettangian, 1688.9 m (1500 +/- 400 ppm CO_2); 1686.9 m (1200 ppm +/- 150 ppm CO_2); *Czekanowskia* sp. 1 - upper Hettangian, 1677.2 m (1300 +/- 100 ppm CO_2); *Baiera* sp. 1 (lower Sinemurian, 1624.9 m – 1500 +/- 100 ppm CO_2) and *Baiera* sp. 4 (upper Pliensbachian, 1276 m – 1200 +/- 150 ppm CO_2). The varied measurement error depends on the size and preservation quality of the measured cuticle surfaces. The difference between the two last samples shows a marked decrease of pCO_2, from a high value in the early Sinemurian to much lower value in the Late Pliensbachian (Fig. 7). For the Hettangian, our results fit the other results obtained in other studies, where pCO_2 varied from 1000 to 1500 ppm (Barbacka 2011), following high 2000-2500 ppm at the T/J boundary (Steinthorsdottir et al 2011). Similar values are given in the compilation of Foster et al. (2017), where CO_2 remains above 1000 ppm for Hettangian and Sinemurian. For the Late Pliensbachian, the single obtained value of c. 1200 pCO_2 from Kaszewy is the highest hitherto

reported. For this age there were values given by Xie et al (2006) of c. 940 ppm or c. 900 ppm, but these values were calculated from a different conifer species, which is discussed by Steinthorsdottir and Vajda (2015). More generally, the concentration of c 960 ppm pCO_2 for the Early Jurassic was interpreted also from Swedish (Beerling et al 1998), Danish (McElwain et al 2005 – of note is a wide range between 500 and 2500 ppm for lower Toarcian), Chinese (c. 800 ppm – Chen et al. 2001) and Australian (900 ppm based on araucarialean conifers) material (Steinthorsdottir and Vajda 2015) - see Fig. 7 and discussion by Barbacka (2011). Generally, the differences in SI and pCO_2 calculations are not outstanding: pCO_2 values oscillate within certain range and average values are given. Nevertheless, some inaccuracies are possible, for example pCO_2 can be also influenced by the Carboniferous standardization of NLE, with different authors making different assumptions. The SI and SD of the NLE are used as reference for counting these values for fossil plants. Calibration usually is made empirically in controlled values of CO_2 concentration. Different authors have calibrated *Ginkgo biloba* under different conditions from 300 to 560 ppm which results in fluctuations of calculated pCO_2 values ranging from c. 960 to c. 1500 ppm respectively, which is discussed by Barbacka (2011). Such deviations should appear if differently calibrated NLE are used in the pCO_2 calculation . The results from the Late Hettangian of Kaszewy, calculated from *Baiera* sp. 2, fit within general climatic trends given by Kürschner (2001). We observe that *Czekanowskia* and *Baiera* stomatal density (sensitive to pCO_2 and consequently temperature differences) is generally compatible with $\delta^{13}C_{wood}$, while these genera are not themselves specifically related to a strict range of temperature. Their deciduous character is connected with seasonal temperature and precipitation variations (Fig. 7). Both genera commonly occur together among dominant elements of Siberian-Canadian provinces and are known as mesotemperate plants, characteristic of flood plain/delta peat-forming assemblages (Rees et al 2000). *Czekanowskia* is one of the commonest plants of coal bearing deposits of Siberia, forming wetland forests (Krassilov et al 2003). Commonly regarded as an indicator of temperate climate, in Poland it was found (apart from Kaszewy) in the northern margin of the Holy Cross Mountains (Barbacka et al 2014) together with other Siberian element *Pseudotorellia* Florin (Kürschner 2001). The genus *Baiera* in Poland has been reported from the Holy Cross Mountains and the Lublin Coal Basin (Barbacka et al 2014). In Mesozoic times, *Baiera*, together with other ginkgophytes of similar type (*Ginkgoites*, *Sphenobaiera*) were widespread and were connected with rather stable, warm to temperate climate and humid conditions (Barbacka 2011; Zhou 2009).

5. Carbon cycle and temperature interpretation

The interpretation of the relationship between $\delta^{13}C_{wood}$ and TOC_{cont} must rely on some baseline assumptions. The carbon cycle includes many simultaneous processes with different time scales, involving very complex processes of carbon mass and isotopic fluxes to and out of the ocean–atmosphere system. Concerning the carbon cycle, in particular the fluxes into the atmospheric system, we focus here on processes registered in plant matter (Gröcke 2002). Experimental data from plant growth chambers obtained by Schubert and Jahren (2012), further developed by Cui and Schubert (2016) allowed formulation of a simple model (identified as the C3 proxy) in which plant carbon-isotope composition depends on changes in only two atmospheric variables, i.e. source isotopic composition of carbon dioxide ($\delta^{13}CO_2$) and the pCO_2. However, for $\delta^{13}C$ to be used as an accurate and precise method to reconstruct pCO_2 the major requirement is to demonstrate that changes in CO_2 are the main driver of changes in $\delta^{13}C$. It should be emphasized that only those experiments which are based on C3 plants can be taken in account for the current study, as C4 plants (absent in Triassic - Early Jurassic times) show different fractionation pattern (Diefendorf et al 2010). Source isotopic composition of $\delta^{13}CO_2$ during the Early Jurassic epoch is a complex issue, as carbon released to the atmosphere can have multiple different sources with different $\delta^{13}CO_2$ values, anywhere from -70‰ (gas hydrate) through thermogenic methane (-50 to -7‰), oxic degradation of organic matter (-20 to -30‰) (Them et al 2017a) and volcanic CO_2 (- −6±2‰) (Beerling & Brentnall 2007; Ruebsam et al 2019, 2020; Gales et al 2020). Thus, observed changes to $\delta^{13}C$ of the atmosphere (on the influx side) can be caused by widely varying flux changes of carbon depending on the source, which would have widely varying effects on changes in pCO_2 for the same change in $\delta^{13}C$ - and resulting temperature (one should bear in mind that changes to $\delta^{13}C$ can be caused by changes in carbon sink, such as decreasing organic carbon burial). However, negative carbon isotope excursions of an amplitude of about 3–4‰ observed in the latest Triassic and Early Jurassic can only be produced by emissions of ^{13}C-depleted carbon such as gas hydrates, thermogenic methane or oxic organic matter degradation (Them et al 2017a; Pieńkowski et al 2016; Ruebsam et al 2020) or a mixture of these sources (Pagani et al 2006), because unrealistically high amounts of volcanogenic CO_2 (released in short time – short carbon cycle) would be required to sufficiently affect the isotopic composition of the exchangeable carbon reservoir (Beerling and Brentnall 2007; Ruebsam et al 2020). For example, Heimdal et al (2020) postulate for the latest Rhaetian-earliest Hettangian case that thermogenic carbon generated from the contact aureoles around CAMP sills represented a credible source for the negative CIEs. Concerning short-term fluxes of carbon into the atmosphere-ocean system, volcanogenic emissions (usually prolonged over long periods of time) acted generally rather as a trigger for a cascade of surface carbon cycling processes, mobilizing methane and CO_2 characterized by a more negative $\delta^{13}CO_2$ signature. Thus, fluxes from the shallow sedimentary sources were a major contributor to the growth of pCO_2 with negative ^{13}C signature (e.g. Hesselbo et

al 2000, Them et al 2017 a, Ruebsam et al 2020). Additionally, increasing pCO_2 causes $\delta^{13}C$ negative fractionation by C3 plants and both caused the negative isotopic signal registered in fossil plants (Hare et al 2018). Similarly, enhanced decomposition of continental carbon pool caused by rising temperature has a short-term, strong feedback effect (Pieńkowski et al 2016). The rising pCO_2 was a major factor in raising temperature, and temperature growth led to depletion of TOC_{cont}.

On the other hand, increasing pCO_2, climate warming and enhanced hydrological cycle (causing enhanced delivery of nutrients to the oceans) lead to increased ocean productivity and increased rate of burial of organic carbon, resulting in drawdown and fall in atmospheric pCO_2, and positive excursions in both organic and inorganic carbon (Kump and Arthur 1999). The drawdown of atmospheric CO_2 led to global cooling and higher accumulation of TOC_{cont}.

Significant, moderate or strong (Evans 1996) correlation between $\delta^{13}C_{wood}$ and TOC_{cont} ($r = 0.53 – 0.59$; $Rs = 0.61$; Fig. 5) could likely develop in response to the global carbon cycle (cf. Gröcke et al 1999). While the fluxes of CO_2 with negative $\delta^{13}C$ signature led to rising pCO_2, negative C isotopic signal registered in fossil plants and global warming, massive burial of ^{13}C-depleted organic carbon at a global scale resulted in higher $\delta^{13}C$ values in all carbon cycle reservoirs, and the attendant drawdown of atmospheric CO_2 led to global cooling. As noted by Pieńkowski et al (2016), the variability in TOC_{cont} contents in the Polish late Pliensbachian to early Toarcian successions is interpreted primarily as a reflection of the efficiency of terrestrial biodegradation, which depended particularly on temperature, creating favourable conditions for fungi (Fig. 6) that efficiently degraded the most common and otherwise resistant to degradation land palynomaceral, i.e. wood, composed mainly of lignin (Lopez-Mondejar et al 2018). Increased fungal activity was noted in other periods characterized by elevated temperature, such as Paleocene-Eocene thermal maximum (PETM) – Kender et al (2012). In contrast, lower temperatures slow down fungal-mediated decomposition rates (Feng et al 2008), enhancing terrestrial carbon accumulation. Similar processes connected with accumulation and destruction of soil organic matter are observed in recent experiments involving soil warming leading to decomposition of lignin in soil (Feng et al 2008). It should be noted that bacteria can play some role in wood degradation as well (Blanchette et al., 1990). However, bacterial degradation occurs at a slow rate compared with fungal decay and detritivore fungi are singled out as the only organisms which were able to degrade lignin tissues (Richardson et al 2012). The current study extends the $\delta^{13}C_{wood}$ and TOC_{cont} dataset for Poland to the whole Lower Jurassic series and the late Rhaetian (Figs. 2, 5, 7). If it is assumed that the temperature is the main factor of TOC_{cont} reduction, then we can link the observed relationship between $\delta^{13}C_{wood}$ and TOC_{cont} to the temperature warming-cooling trends, associated with global carbon cycle. An important point is that

this correlation does not demonstrate $\delta^{13}C_{wood}$ – temperature direct causation. In this case, the $\delta^{13}C_{wood}$, temperature and TOC_{cont} would be responding to another forcing (CO_2 fluxes and C_{org} burial, i.e. carbon cycle – cf. Gröcke et al 1999). Additionally, possible influence of sedimentary and diagenetic factors, reflected also as palynofacies inversions (Pieńkowski and Waksmundzka 2009) could alter the TOC_{cont} content. On the other hand, extremely enhanced hydrological cycle at the peaks of T-OAE could have had some impact on the observed $\delta^{13}C_{wood}$ – TOC_{cont} relation, in that organic matter would have been rapidly removed and delivered to the receiving basin before the decomposition processes had fully taken effect. This could be responsible in slightly reversed $\delta^{13}C_{wood}$ – TOC_{cont} trend observed in four Toarcian samples with most negative $\delta^{13}C_{wood}$ values (Fig. 5).

Weaker correlation in the entirely continental Rhaetian section can be explained by much stronger impact of local environmental factors, influencing strongly differentiated TOC_{cont} sequestration that is facies specific in space and time, for example fluvial plain/lacustrine shifts of environments. In contrast, most of the Lower Jurassic strata were deposited in marginal-marine/deltaic environments, where the TOC_{cont} content was averaged in sedimentary processes. Thus, results obtained from these settings show fewer outliers.

Inferred latest Triassic-Early Jurassic temperature trends for the c. 40°N paleolatitude are shown in stratigraphical order in the Fig. 7. As shown by floral remains, the temperatures were generally temperate to warm, with a slight decreasing trend over time, punctuated by two marked hotter periods – in the Late Rhaetian and in particular in the early Toarcian, during the Toarcian Oceanic Anoxic Event Carbon Isotope Excursion (T-OAE CIE), when temperatures peaked. Several less marked periods of temperature rise were indicated in the Hettangian (*planorbis*, *liasicus*), Sinemurian (*turneri* – confirmed also by Schöllhorn et al 2020 and Hesselbo et al 2020a), *oxynotum* – see also Riding et al 2013) and Pliensbachian (*davoei*); the latter reported by several authors, e.g. Dera et al (2011); Gomez et al (2015); Price et al (2016); Peti and Thibault (2017). Lower temperatures occurred in the latest Rhaetian/earliest Hettangian, late Hettangian (periodically), early Pliensbachian (*jamesoni-brevispina*) and particularly in the Late Pliensbachian (*stokesi*, *gibbosus*, *spinatum*), which seems to be the coolest period in the Early Jurassic, confirmed in many papers (Price 1999; Korte and Hesselbo 2011; Dera et al, 2009, 2011). This cooler interval was punctuated by a short-lived warming episode at the *margaritatus*/*spinatum* boundary. Of note are relatively frequent inferred temperature shifts in the late Rhaetian and the late Hettangian, which can be attributed to the methane releases from clathrates or wetlands, triggered by peaks of volcanic activity of the Central Atlantic Magmatic Province (Palfy et al, 2001; Hesselbo et al 2002; Blackburn et al 2013) or by thermogenic carbon generated from the contact aureoles around CAMP sills (e.g., Heimdal et al 2020). Rapid climate shifts (inferred from clay mineral composition) in the late Rhaetian and possibly earliest Hettangian

with marked cool and dry episodes was postulated as one of the possible scenarios of the end-Triassic mass extinction on continents (Pieńkowski et al 2014). Similar contrasting temperature shifts are observed in the early Toarcian, when the T-OAE CIE and coeval greenhouse period might have been immediately preceded and followed by relatively cooler intervals (middle *tenuicostatum* and mid-*serpentinumfalciferum/serpentinum* pessima) – Mc Elwain et al (2009), although some reports point to continuity of warm conditions long after the T-OAE (Hermoso and Pellenard 2014). It should be pointed out, that the post-*falciferum* Toarcian sediments in Kaszewy and the whole Polish basin (Pieńkowski 2004; Hesselbo and Pieńkowski 2011) are poorly constrained in stratigraphic terms, as there is a major sequence boundary occurring somewhere in the upper *falciferum/serpentinum* zone with ensuing sedimentation of almost homogenous sandstone interval. Generally, obtained temperature trends are broadly similar to the trends interpreted by Dera et al (2009, 2011). The inferred temperature trends are compared with independently obtained SI results, reflecting pCO_2 in the atmosphere, which should have reflected annual mean air temperature fluctuations in the atmosphere. Although only six pCO_2 measurement points were possible, four measurements came from relatively narrow upper Hettangian interval, enabling comparison with corresponding $\delta^{13}C_{wood}$ results. Additionally, more SI results come from McElwain et al (2005) and Steinthorsdottir et al. (2011) – Fig. 7. The general pCO_2/temperature trends inferred from SI correspond with the $\delta^{13}C_{wood}$ changes (Fig. 7).

6. Variables influencing $\delta^{13}C_{wood}$ and TOC_{cont} - discussion

The $\delta^{13}C_{wood}$ of plant matter in the geological record would be generally dependent on the $\delta^{13}C$ of the palaeoatmosphere (Hasegawa 1997; Hesselbo and Pieńkowski 2011; Schubert and Jahren 2012; Cui and Schubert 2016; Pieńkowski et al 2016; Them et al 2017b; Hare et al 2018; Ruebsam et al 2020). Moreover, a parallel stratigraphic evolution between terrestrial and marine organic matter-$\delta^{13}C$ (e.g. Hesselbo and Pieńkowski 2011; Them et al 2017b; Storm et al., 2020) strengthens the hypothesis that changes in the carbon isotope curve are a genuine feature reflecting the global carbon cycle and change in $\delta^{13}C$ of atmospheric CO_2. From an ecophysiological standpoint changes in $\delta^{13}C$ are also linked to changes in water use efficiency of the plants, therefore Lomax et al (2019) regarded that the model of Schubert and Jahren (2012) and Cui and Schubert (2016) is only operable over a limited climate space. Indeed, mean annual precipitation (MAP) can affect carbon isotope fractionation in plant materials, whereby $\delta^{13}C$ values are negatively correlated with MAP in extant and fossil C3 plant (Diefendorf et al 2010; Kohn, 2010; Hare et al, 2018). However, differences in fractionation caused by MAP are significant (over 2 ‰) only when the most contrasting plant habitats are compared - dry (< 600 mm/year) and very humid (> 2000 mm/year) MAP (Diefendorf et

al 2010; Kohn 2010). Moreover, Hare et al (2018) showed that the contributions from changing MAP are insignificant when compared to the effect of pCO_2 for C3 plants. Influence of mean annual precipitation (MAP) within a relatively stable climatic belt is regarded as generally insignificant (Hare et al 2018), although some intermittent increases of MAP (particularly during the Toarcian Oceanic Anoxic Event; Hesselbo et al 2007; Pieńkowski and Waksmundzka 2009; Hesselbo and Pieńkowski 2011; Pieńkowski et al 2016) might have had a minor impact on observed $\delta^{13}C_{wood}$ values. Rodriguez et al (2019) attributed the difference observed between $\delta^{13}C_{cont}$ in the Southern Tethyan and Iberian margin (semi-arid climate belt) and the Polish Basin (winter wet/warm climate belt) to the $\delta^{13}C$ fractionation caused by difference in MAP, but still this averaged difference does not exceed 1‰, even if this was a time of Toarcian Oceanic Anoxic Event characterized by much enhanced climatic contrasts. Studies on the Toarcian compound-specific carbon isotope data of land plant wax lipids have suggested that changes in $\delta^{13}C$ n-alkane vary as a function of changes in the atmospheric CO_2 concentration (Schouten et al 2000; Ruebsam et al 2020). Fractionation of $\delta^{13}CO_2$ by C3 plants due to increasing pCO_2 would amplify the observed overall $\delta^{13}C_{wood}$ values, and increased pCO_2 would result in temperature rise and subsequent reduction of TOC_{cont}. Interestingly, there is also a direct positive feedback between elevated atmospheric CO_2 concentrations and soil organic matter decomposition (Wolf et al 2007). Fractionation by different plant organs related to different plant taxa or seasonal precipitation changes should also be considered. However, any sample of wood material analysed herein would also contain averaged isotopic signals spanning tens, hundreds or thousands of years – averaging out specific fractionation factor of the originating plant taxon, or the part of the plant from where the wood comes. This conclusion is supported by the common observation of parallel stratigraphic trends in $\delta^{13}C_{wood}$ values and $\delta^{13}C$ of bulk marine organic matter (e.g. example of Toarcian of Lusitanian Basin (Hesselbo et al. 2007, Fantasia et al. 2019). It should be also noted that only the Coniferales and Ginkgophyta produced significant amounts of secondary xylem and most of our wood likely came from conifer trees (Morgans 1999; Philippe et al 2006; Pieńkowski et al 2016). The amount of TOC_{cont} could be also controlled by the rates of production, not only degradation. However, if production rate were the significant controlling factor, then we should expect maximum concentrations of TOC_{cont} during the periods characterized by highest humidity, pCO_2 and, consequently, productivity (e.g. T-OAE – Pieńkowski et al. 2016). However, the situation is exactly opposite and TOC_{cont} is very low during T-OAE, most likely due to a rapid decomposition (Figs. 2, 6). Another factor which could influence TOC concentration is the sedimentation rate – the higher it is, the lower TOC concentration should be. However, the highest overall sedimentation rate occurred in Hettangian, where the average TOC_{cont} content is highest (Fig. 2). Constraints on the late Rhaetian and Early Jurassic environment in Poland based on reconstruction of the hydrological cycle, standing vegetation and clay mineral analysis (Hesselbo and Pieńkowski 2011; Brański 2009, 2012; Pieńkowski

et al 2012, 2014, 2016) does not indicate the presence of dry or semi-dry habitats, except for short periods in the late Rhaetian (these samples were excluded from our $\delta^{13}C_{wood}$-TOC_{cont} considerations). Macrophyte remains in Kaszewy (Fig. 7) and hitherto analysed palynomorphs in the late Rhaetian and Early Jurassic time interval (Pieńkowski and Waksmundzka 2009; Pieńkowski et al 2012; Pieńkowski et al 2016) point to generally stable climate zone and relatively stable mean annual precipitation (MAP). Annual sensitivity values for the Lower Jurassic woods from similar paleolatitude of Yorkshire, UK (Morgans 1999) generally fall into the 'complacent' field, suggesting little interannual perturbation and mostly uniform growing conditions, with weak to moderate seasonality. Our material comes from the same latitudinal zone of changing humidity, but not drastically enough to cause any significant $\delta^{13}C$ fractionation in C3 plants (Diefendorf et al 2010; Kohn 2010; Hare et al 2018).

Humidity-related fractionation effects could thus only slightly modulate the observed C isotope trends (for example during T-OAE, when floristic and palynological proxies indicate increased humidity; Pieńkowski et al 2016), rather than being the significant factor, or change systematically in conjunction with pCO_2, thus indirectly amplifying rather than destroying the observed relationship. It should be noted that based on spore-pollen assemblages from marine strata of Yorkshire, UK, Slater et al (2019) postulated extreme seasonal conditions for the T-OAE time interval with an increase of warm- and even drought-adapted plants through the CIE interval. Notably, their palynodiagram (their fig. 2) shows lack or a minimum content of bryophyte and lycophyte spores through the Toarcian, in particular during the T-OAE. However, data from the Polish basin, located approximately at the same paleolatitude, show prominent and continuous share of spores and megaspores produced by extremely hydrophilic lycophyte (e.g. quill worts) through the T-OAE (Marcinkiewicz 1962, 1971; Pieńkowski and Waksmundzka 2009; Hesselbo and Pieńkowski 2011; Pieńkowski et al 2016). As the Polish material comes from coastal/deltaic sediments, it should better reflect standing vegetation in the hinterland than open marine settings in Yorkshire. Thus, it is still possible that the bryophyte and lycophyte spores (megaspores in particular) and much of fern spores were eliminated from the Yorkshire material by taphonomic processes. In our opinion, Slater's et al (2019) interpretation of extremely wet/dry seasons should be relaxed in favor of more humid conditions enabling the survival of extremely hydrophilic plants.

Plant chamber experiments have also revealed relationships between carbon isotope discrimination and changing pO_2 (Porter et al 2017), but this variable in the geological record is interpreted from reconstructions which vary widely, particularly for the Mesozoic and early Cenozoic eras (Glasspool and Scott 2010). In respect to the geological time interval studied herein, these low-

resolution models are often controversial, although they confirm a general rule that high rates of organic carbon burial results in subsequent oxygen production (Krause et al 2018).

The described herein $\delta^{13}C_{wood}/TOC_{cont}$ relationship is surprising. However, if the correlation is so significant, it follows that there is a natural reason for it. There is also a relationship between terrestrial TOC and temperature from actualistic experimental work. As we wrote above, decomposition of soil labile carbon is highly sensitive to temperature variation and elevated pCO_2 resulting in higher temperature could be conducive for enhanced soil organic matter decomposition (Fang et al 2005; Feng et al 2008; Pieńkowski et al 2016; López-Mondéjar 2018). The continental kerogen studied herein had likely been oxidized on land or in rivers and before delivery to the receiving basin – remineralization of TOC_{cont} in a marginal-marine basin was possible, but among different continental types of organic matter, the wood and charcoal was least affected by degradation in the basin (Pieńkowski and Waksmundzka 2009). Even the most critical approaches (Davidson and Janssens 2006) admit that despite controversies, the observational data are converging to demonstrate that irrespective of labile or recalcitrant character, the soil carbon pool decomposes with apparent detectable temperature sensitivity (Fang et al 2005; Feng et al 2008). Wood is known to react more to higher temperature changes (kinetic theory), which can explain why the population of samples with more diversified $\delta^{13}C_{wood}$ and TOC_{cont} values (e.g. Toarcian) shows relatively higher coefficiency in $\delta^{13}C_{wood}$/ TOC_{cont} function (Fig. 5).

Considering the above argument, it should be noted that some emerging reports from Lower Jurassic marine sediments (Hesselbo et al 2020b; Ullmann et al 2020) demonstrate a lack of correlation between $\delta^{13}C_{org}$ and $\delta^{18}O$ (reflecting in general, although still debatably, sea-water temperature) in some sections, for example the lower Sinemurian in UK or the Toarcian in Iberia. However, Schöllhorn et al (2020) show good convergence between these two variables in Sinemurian of Dorset (UK), while there are divergences in the lower Pliensbachian. Of note is also the fact that Hesselbo et al. (2020a,b) point to divergence in the lower Sinemurian, while the Hettangian part shows rather good convergence between the two variables. Similarly, Price et al. (2016) compared $\delta^{13}C$ and $\delta^{18}O$ for the Sinemurian and Pliensbachian section in Dorset and there is a generally good convergence for most of the section, but in some parts of the profile one can observe some divergences as well. There is good convergence of $\delta^{13}C$ and $\delta^{18}O$ both in the Rhaetian-Hettangian sections in SW UK (Korte et al. 2009) and in the uppermost Pliensbachian – lower Toarcian section in the Peniche GSSP profile in Portugal (Suan et al. 2008; Fantasia et al. 2019). Nevertheless, existing $\delta^{13}C$ and $\delta^{18}O$ divergences tend to cast some doubts, at least on universality of $\delta^{13}C_{org}$ and $\delta^{18}O$/temperature relations because one should expect even stronger relationship between these parameters in marine sediments than there is between $\delta^{13}C_{wood}$ and marine temperature, as the

relationship is more direct. However, there are some inherent uncertainties regarding $\delta^{13}C$ and $\delta^{18}O$ results from marine deposits and their interpretation. It is now well established that bulk organic C-isotope records need to be regarded with caution due to the mixing effects of different types of carbon, each with their own $\delta^{13}C$ signature (Van de Schootbrugge et al. 2008; Suan et al. 2015; Schöllhorn et al. 2020). In Kaszewy these problems are avoided, because the $\delta^{13}C_{wood}$ values comes from homogenous material. The other question is the possible influence of oceanographic processes, acting (at least partly) independently from global atmospheric pCO_2 and temperature changes. Opening of the Hispanic corridor in Sinemurian and its widening in Pliensbachian (Porter et al. 2013) impacted oceanic circulation, marine faunal exchange pattern and, very probably, also isotopic and temperature pattern in the Jurassic seaways of the European area.

The current paper supports and extends similar results obtained from the late Pliensbachian-early Toarcian deposits of the Polish basin (Pieńkowski et al. 2016) and this is a first attempt to infer a continuous record of air temperature trends through such a long period of geological time. Independently obtained trends of interpreted palaeotemperatures are juxtaposed with data from stomatal index which are thought to represent changes in pCO_2. It seems that the proposed relationship works as a temperature signal only for a warm/winter-wet climatic zone. The $\delta^{13}C_{wood}$/ TOC_{cont} trend observed in the semi-arid climate belt seems to be different, at least during the Late Pliensbachian-early Toarcian interval in the Southern Tethyan and Iberian margin (Rodriguez et al 2019). It is possible that during the T-OAE the Southern Tethyan and Iberian margin was influenced by the adjacent tropical climatic zone, which caused the observed differences. Of note is also modeling of major carbon cycle perturbations around the Triassic-Jurassic boundary, showing coincidence between $\delta^{13}C$ and pCO_2 changes (Heimdal et al. 2020).

7. Conclusions

1. There is an observed highly significant relationship between $\delta^{13}C_{wood}$ and TOC_{cont} in the Rhaetian/Lower Jurassic from Kaszewy that can be defined by an equation. The premise is that in mid-latitudes, a controlling factor on the relation between $\delta^{13}C_{wood}$ and preservation of continental total organic carbon (TOC_{cont}) is the efficiency of terrestrial biodegradation which is pCO_2 and temperature dependent, although there are several factors that control both $\delta^{13}C_{wood}$ and TOC_{cont}.

2. The $\delta^{13}CO_2$ of the Rhaetian and Early Jurassic was largely controlled by $\delta^{13}C$-depleted fluxes in and out of the ocean-atmosphere system. Likely, there is are non-causal correlations between $\delta^{13}C_{wood}$, TOC_{cont} and temperature trends. Such correlations may develop because massive fluxes into the ocean-atmosphere system and subsequent burial of ^{13}C-depleted organic carbon (flux out of the

ocean-atmosphere system), at a global scale results in global warming and cooling episodes, registered in the continental carbon pool as $\delta^{13}C_{wood}$ and TOC_{cont} fluctuations.

3. The relationship between $\delta^{13}C_{wood}$ and TOC_{cont} can hypothetically be be useful, even if non-causal, for ~25 Myr long latest Rhaetian and Early Jurassic air temperature interpretation at c. 40°N paleolatitude. However, its utility depends on how strong the carbon cycle signal is, and how many other influences have operated on the system.

4. Independently obtained trends of interpreted palaeotemperatures were juxtaposed with data from stomatal index which are thought to represent changes in pCO_2, and results obtained from stomatal index calculations are compatible with the interpreted temperature trends.

5. In our material, deposits of coastal/deltaic environments are most suitable for studying the relationship between carbon-isotopes, continental TOC, and temperature, because these facies contain more representative, averaged material delivered from a large catchment areas – in contrast to alluvial plains where TOC is dependent on a more localized fluvial setting.

6. Unique, expanded and continuous cores from Kaszewy and Mochras allowed reliable $\delta^{13}C$ chemostratigraphic correlation of marine and marginal/non-marine Lower Jurassic deposits.

7. While this study suggests an overall implication for Earth system studies and offers potentially independent means (registered in the continental carbon pool) to estimate latest Triassic to Early Jurassic atmospheric temperatures, the relationship between TOC_{cont}, $\delta^{13}C_{wood}$ and temperature should be further tested and treated as still hypothetical because in general organic carbon isotope records are potentially subject to many different influences.

Acknowledgements

We thank Przemysław Karcz and Marcin Janas for performing RockEval 6 pyrolithic analyses. We thank Marta Hodbod and dr Marta Waksmundzka for palynomaceral separation and identification of palynomorphs. Peter Ditchfield (Oxford) is thanked for C-isotope analysis. We are grateful to the PGE Company for granting access to the core and agreeing to take samples. We are grateful to Professor Thomas Algeo, guest editor of this volume, managing editors Professors Shane Schoepfer and Alessandra Negri, and two anonymous Reviewers for their valuable comments which improved the paper. This paper is financed (G.P., M.B.) from resources of the Polish National Science Centre, granted on the basis of decisions no. DEC-2012/06/M/ST10/00478, no2017/25/B/ST10/02235 and no. 2017/25/B/ST10/01273. This is a contribution to the ICDP and NERC project JET (grant number NE/N018508/1) and IGCP project 632 “Continental Crises of the Jurassic”.

References

Baker, S. J., Hesselbo, S. P., Lenton, T. M., Duarte, L. V., Belcher, C.M., 2017. Charcoal evidence that rising atmospheric oxygen terminated Early Jurassic ocean anoxia. Nat. Commun. 8: 15018, DOI: 10.1038/ncomms15018

Barbacka, M. 2011. Biodiversity and The Reconstruction of Early Jurassic flora from the Mecsek Mountains (S. Hungary). Acta Palaeobot. 51,127-179

Barbacka, M., Pacyna, G., Feldman Olszewska, A., Ziaja, J., Bodor, E. 2014. Triassic-Jurassic flora of Poland; floristical support of climatic changes. Acta Geol. Pol., 64, 281–308

Barbacka, M., Püspöki, Z., Bodor, E., Forgács, Z., Hámor-Vidó, M., Pacyna, G., Mcintosh, R.W. 2015. Palaeotopography related plant succession stages in a coal forming deltaic succession in early Jurassic in Hungary. Palaeogeogr., Palaeoclimat., Palaeoecol. 440, 379-393.

Barbacka, M., Popa, M.E., Mitka, J., Bodor, E., Püspöki, Z., Mcintosh, R.W. 2016. A quantitative approach for identifying plant ecogroups in the Romanian Early Jurassic terrestrial vegetation. Palaeogeogr., Palaeoclimatol., Palaeoecol. 446, 44–54.

Barth, G., Franz, M., Heunisch, C., Kustatsche, E., Thies, D., Vespermann, J. and Wolfgramm, M., 2014. Late Triassic (Norian-Rhaetian) brackish to freshwater habitats at a fluvial-dominated delta plain (Seinstedt, Lower Saxony, Germany). Palaeobio., Palaeoenv. 94:495–528; DOI 10.1007/s12549-014-0168-6

Barth, G., Franz, M, Heunisch, C., Ernst, W., Zimmermann, J., Wolfgramm, M. 2018. Marine and terrestrial sedimentation across the T–J transition in the North German Basin. Palaeogeogr., Palaeoclimatol., Palaeoecol. 489, 74-94

Barth, G., Pieńkowski, G., Zimmermann, J., Franz, M., Kuhlmann, G., 2018. Palaeogeographical evolution of the Lower Jurassic: high-resolution biostratigraphy and sequence stratigraphy in the Central European Basin. In: Williams, B., Kukla, P. A., Mazur, S., McKie, T., Mijnlieff, H. F. & Van Ojik, K. (eds) Mesozoic Resource Potential in the Southern Permian Basin. Geological Society, London, Sp. Publ., 469, https://doi.org/10.1144/SP469.8

Bartolini, A., Guex, J., Spangenberg, J.E., Schoene, B., Taylor, D.G., Schaltegger, U., Atudorei, V., 2012. Disentangling the Hettangian carbon isotope record: implications for the aftermath of the end-Triassic mass extinction. Geochem., Geophys., Geosyst., 13 (1), doi:10.1029/2011GC003807

Beerling, D.J. 1999. Stomatal density and index: theory and application. In: Jones T.P. & Rowe N.P. (eds), Fossil plants and spores: modern techniques. The Geol. Soc., London: 251–256.

Beerling, D.J., McElwain, J.C., Osborne, C.P. 1998. Stomatal response of the “living fossil” *Ginkgo biloba* L. to changes in atmospheric CO_2 concentrations. J. Exp. Bot., 49, 1603–1607.

Beerling, D.J. & Royer, D.L. 2002a. Fossil plants as indicators of the Phanerozoic global carbon cycle. Ann. Rev. Earth Planet. Sci., 30: 527–556.

Beerling, D.J. & Royer, D.L. 2002b. Reading a CO_2 signal from fossil stomata. New Phytologist, 153, 387–397.

Beerling, D. J., Brentnall, S. J. 2007. Numerical evaluation of mechanisms driving Early Jurassic changes in global carbon cycling. Geology 36, 231–234

Berner, R.A., Kothavala, Z. 2001. Geocarb III: A revised model of atmospheric CO2 over Phanerozoic time. Am. Journ. Sci. 301, 182–204.

Blackburn, T.J., Olsen, P.E., Bowring, S.A., McLean, N.M., Kent, D.V., Puffer, J., McHone, G., Rasbury, E.T., Et-Touhami, M., 2013. Zircon U-Pb geochronology links the end-Triassic extinction with the Central Atlantic Magmatic Province. Science 340, 941–945

Bougeault, C., Pellenard, P., Deconinck, J.-F., Hesselbo, S.P., Dommergues, J.-L., Bruneau, L., Cocquerez, T., Laffont, R., Huret, E., Thibault, N. 2017. Climatic and palaeoceanographic changes during the Pliensbachian (Early Jurassic) inferred from clay mineralogy and stable isotope (C–O) geochemistry (NW Europe). Glob. Planet. Change 149, 139–157.

Brański, P. 2009. Influence of palaeoclimate and the greenhouse effect on Hettangian clay mineral assemblages (Holy Cross Mts. area, Polish Basin). Geol. Quart. 53, 363–368.

Brański, P., 2012. The mineralogical record of the Early Toarcian stepwise climate changes and other environmental variations (Ciechocinek Formation, Polish Basin). Vol. Jurassica 10, 1–24.

Chen, L.Q., Cheng-Sen, Li, Chaloner, W.G., Beerling, D.J., Sun, Q.G., Collinson, M.E., Mitchell, P.L. 2001. Assessing the potential for the stomatal characters of extant and fossil Ginkgo leaves to signal atmospheric CO2 change. Am. Jour. Bot., 88, 1309–1315.

Cohen A.S, Coe, AL, Harding, S.M, Schwark, L., 2004. Osmium isotope evidence for the regulation of atmospheric CO2 by continental weathering. Geology 32, 157–160

Cui, Y., Schubert, B. A., 2016. Quantifying uncertainty of past pCO_2 determined from changes in C3 plant carbon isotope fractionation. Geochim. Cosmochim. Acta 172, 127–138

Dadlez, R., 1973. Jura dolna. In: Krośniewice IG 1 (ed. S . Marek). Profile Głębokich Otworów Wiertniczych Instytutu Geologicznego 5, 38–43

Dadlez, R. (ed.), 1998. Mapa tektoniczna kompleksu cechsztyńsko-mezozoicznego na Niżu Polskim w skali 1:500 000. PGI, Warszawa

Dadlez, R., 2003, Mesozoic thickness pattern in the Mid-Polish Trough: Geol. Quart. 47, 223–240

Dadlez, R., Kopik, J. 1972. Selected problems of Liassic stratigraphy and sedimentation in the area between Świnoujście and Gryfice (North-West Poland). Kwartalnik Geol.16, 620–637

Dadlez, R., Marek, S., Pokorski, J. (eds) 1998. Palaeographical Atlas of the Epicontinental Permian and Mesozoic in Poland (1:2 500 000). Polish Geological Institute, Warszawa

Davidson, E. A., Janssens, I. A. 2006. Temperature sensitivity of soil carbon decomposition and feedbacks to climate change. Nature 440, 165–173

De Lena, L., Taylor, D., Guex, J., Bartolini, A., Adatte, T., van Acken, D., Spangenberg, J.E., Samankassou, E., Vennemann, T., & Schaltegger U., 2019. The driving mechanisms of the carbon cycle perturbations in the late Pliensbachian (Early Jurassic). Sci. Rep. 9, 18430

Dera, G., Pellenard, P., Neige,P., Deconinck , J.F., Pucéat, E., Dommergues, J.L., 2009. Distribution of clay minerals in Early Jurassic Peritethyan seas: Palaeoclimatic significance inferred from multiproxy comparisons. Palaeogeogr., Palaeoclimatol., Palaeoecol., 271, 39–51

Dera, G., Brigaud, B., Monna F., Laffont, R., Pucéat, E., Deconinck, J.F., Pellenard, P., Joachimski, M.M. & Durlet, C. 2011. Climatic ups and downs in a disturbed Jurassic world. Geology 39, 215–218.

Diefendorf, A.F., Mueller, K.E., Wing, S.L., Koch, P.L., Freeman, K.H., 2010. Global patterns in leaf 13C discrimination and implications for studies of past and future climate. Proc. Natl. Acad. Sci. U.S.A. 107, 5738–5743

Erdei, B., Utescher, T., Hably, L., Tamás, J., Roth-Nebelsick, A., Grein, M. 2012. Early Oligocene Continental Climate of the Palaeogene Basin (Hungary and Slovenia) and the surrounding area. Turkish J. of Earth Sci. 21, 153-186

Evans, J. D., 1996. Straightforward statistics for the behavioral sciences. Pacific Grove, CA: Brooks/Cole Publishing.

Fang, C., Smith, P., Moncrieff, J.B., Smith, J.U., 2005. Similar response of labile and resistant soil organic matter pools to changes in temperature. Nature, 433, 57–59.

Fantasia, A., Adatte, T., Spangenberg, J. E., Font, E., Duarte, L. V., Föllmi, K. B., 2019. Global versus local processes during the Pliensbachian–Toarcian transition at the Peniche GSSP, Portugal: A multi-proxy record, Earth Sci. Rev. 198, 102932.

Feng, X., Simpson, A. J., Wilson, K. P., Williams, D. D., Simpson, M. J.2008. Increased cuticular carbon sequestration and lignin oxidation in response to soil warming. Nat. Geosci. 1, 836–839

Foster, G. L., Royer D. L., Lunt D. J. (2017) Future climate forcing potentially without precedent in the last 420 million years. Nat. Comm. 8, 14845.

Glasspool, I.J., Scott, A.C. 2010. Phanerozoic concentrations of atmospheric oxygen reconstructed from sedimentary charcoal. Nat. Geosci. 3, 627–630

Hare, V.J., Loftus, E, Amy Jeffrey, A., Ramsey, C.B., 2018. Atmospheric CO_2 effect on stable carbon isotope composition of terrestrial fossil archives. Nat. Comm. 9, 252, DOI: 10.1038/s41467-017-02691-x

Hedges, J.I, Keil, R.G., Benner, R. 1997. What happens to terrestrial organic matter in the ocean? Org. Geochem. 27, 195-212

Heimdal, T.H., Jones, M.T., Svensen, H.H. 2020. Thermogenic carbon release from the Central Atlanticmagmatic province caused major end-Triassic carbon cycle perturbations. Proc. Nat. Acad. Sci. U.S.A. doi/10.1073/pnas.2000095117

Gales, E., Black, B., Elkins-Tanton, L.T. 2020. Carbonatites as a record of the carbon isotope composition of large igneous province outgassing. Earth and Planetary Science Letters 535:116076. DOI: 10.1016/j.epsl.2020.116076

Gómez, J.J., Comas-Rengifo, M.J., Goy, A., 2016. The hydrocarbon source rocks of the Pliensbachian (Early Jurassic) in the Asturian Basin (northern Spain): Their relationship with the palaeoclimatic oscillations and gamma-ray response. J. Iber. Geol. 42, 259-273

Gröcke, D.R. 2002. The carbon isotope composition of ancient CO_2 based on higher-plant organic matter. Phil. Trans. R. Soc. Lond. A, 360, 633–658.

Gröcke, D.R., Hesselbo, S.P., Jenkyns, H.C. 1999. Carbon-isotope composition of Lower Cretaceous fossil wood: Ocean-atmosphere chemistry and relation to sea-level change. Geology 27, 155–158

Guex, J., Pilet, S., Müntener, O., Bartolini, A., Spangenberg, J., Schoene, B., Sell, B. Schaltegger, U., 2016. Thermal erosion of cratonic lithosphere as a potential trigger for mass-extinction. Sci. Rep., 6, 23168, doi: 10.1038/srep23168 (2016).

Hallam, A. 2001. A review of the broad pattern of Jurassic sea-level changes and their possible causes in the light of current knowledge. Palaeogeogr., Palaeoclimatol., Palaeoecol. 147, 23–37

Harazim, D., van de Schootbrugge, B., Sorichter, K., Hesig, J., Weug, A., Suan, G., Oschmann, W., 2013. Spatial variability of watermass conditions within the European Epicontinental Seaway during the Early Jurassic (Pliensbachian–Toarcian). Sedimentology 60, 359–390

Hasegawa, T., 1997, Cenomanian–Turonian carbon isotope events recorded in terrestrial organic matter from northern Japan: Palaeogeogr., Palaeoclimatol., Palaeoecol. 130, 251-273.

Haworth, M., Raschi, A. 2014. An assessment of the use of epidermal micro-morphological features to estimate leaf economics of Late Triassic–Early Jurassic fossil Ginkgoales. Rev. Palaeobot. Palynol. 205, 1–8.

Hermoso, M., Pellenard, P., 2014. Continental weathering and climatic changes inferred from clay mineralogy and paired carbon isotopes across the early to middle Toarcian in the Paris Basin. Palaeogeogr., Palaeoclimatol., Palaeoecol. 399, 385–393.

Hesselbo, S.P., Jenkyns, H.C., 1998. British Lower Jurassic sequence stratigraphy. In: de Graciansky, P.C., Hardenbol, J., Jacquin, T., Farley, M., and Vail, P.R. (eds), Mesozoic–Cenozoic Sequence Stratigraphy of European Basins, Sp. Publ. Soc. Sed. Geol. 60, 561–581.

Hesselbo, S.P., Gröcke, D.R., Jenkyns, H.C., Bjerrum, C.J., Farrimond, P.L., Morgans-Bell, H.S., Green, O., 2000. Massive dissociation of gas hydrates during a Jurassic Oceanic Anoxic Event. Nature 406, 392–395.

Hesselbo, S.P., Robinson, S.A., Surlyk, F., 2004. Sea-level changes and facies development across potential Triassic-Jurassic boundary horizons, SW Britain. J. Geol. Soc. Lond. 161, 365–379.

Hesselbo, S.P., Robinson, S.A., Surlyk, F., Piasecki, S., 2002. Terrestrial and marine extinction at the Triassic–Jurassic boundary synchronized with major carbon-cycle perturbation: a link to initiation of massive volcanism? Geology 30, 251–254.

Hesselbo, S.P., Jenkyns, H.C., Duarte, L.V., Oliveira, L.C.V., 2007. Carbon-isotope record of the Early Jurassic (Toarcian) Oceanic Anoxic Event from fossil wood and marine carbonate (Lusitanian Basin, Portugal). Earth Planet. Sci. Lett. 253, 455–470. doi:10.1016/j.epsl.2006.11.009

Hesselbo, S.P., Pieńkowski, G., 2011. Stepwise atmospheric carbon-isotope excursion during the Toarcian Oceanic Anoxic Event (Early Jurassic, Polish Basin). Earth Planet. Sci. Lett. 301, 365–372.

Hesselbo, S. P., Bjerrum, C. J., Hinnov, L. A., MacNiocaill, C., Miller, K. G., Riding, J. B., van de Schootbrugge, B., and the Mochras Revisited Science Team, 2013. Mochras borehole revisited: a new global standard for Early Jurassic Earth history. Scientific Drilling, 16, 81–91; www.sci-dril.net/16/81/2013/

Hesselbo, S.P., Hudson, A.J.L, Huggett, J.M., Leng, M.J., Riding, J.B., Ullmann, C.V., 2020a. Palynological, geochemical, and mineralogical characteristics of the Early Jurassic Liasidium Event in the Cleveland Basin, Yorkshire, UK. Newsletters on Stratigraphy, 53, 191–211.

Hesselbo, S.P., Korte, C., Ullmann, C.V., Ebbesen, A., 2020b. Carbon and oxygen isotope records from the southern Eurasian Seaway following the Triassic Jurassic boundary: parallel long-term enhanced carbon burial and seawater warming. Earth Sci. Rev. 203, 103-131

Hillebrandt, A.V., Krystyn, L., Kürschner, W.M., Bonis, N.R., Ruhl, M., Richoz, S., Schobben, M.A.N., Urlichs, M., Bown, P. R., Kment, K., McRoberts, C.A., Simms, M., Tomãsových, A., 2013. The Global Stratotype Sections and Point (GSSP) for the base of the Jurassic System at Kuhjoch (Karwendel Mountains, Northern Calcareous Alps, Tyrol, Austria). Episodes 36, 162–198.

Howarth M.K., Donovan D.T., 1964. Ammonites of the Liassic family Juraphyllitidae in Britain. Palaeontology 7, 286–305.

Jenkyns, H.C., 1988. The Early Toarcian (Jurassic) anoxic event – stratigraphic, sedimentary, and geochemical evidence. Am. J. Sci. 288, 101–151.

Jones, T.P. & Rowe N.P. (eds), 1999. Fossil Plants and Spores. Modern Techniques. Geol. Soc. London.

Katz, M.E., T, Wright, J.D., Miller, K.G., Cramer, B.S., Fennel, K., Falkowski, P.G., 2005. Biological overprint of the geological carbon cycle. Marine Geology 217, 323–338

Kemp, D.B., Selby, D., and Izumi, K., 2020, Direct coupling between carbon release and weathering during the Toarcian oceanic anoxic event: Geology, v. 48, https://doi.org/10.1130/G47509.1

Kender, S., Stephenson, M.H., Riding, J.B., Leng, M.J., Knox, R.W.O'B., Peck, V.L., Kendrick, C.P., Ellis, M.A., Vane, C.H., Jamieson, R. 2012. Marine and terrestrial environmental changes in NW Europe preceding carbon release at the Paleocene–Eocene transition. Earth Planet. Sci. Lett. 353–354, 108–120

Kohn, M. J. 2010. Carbon isotope compositions of terrestrial C3 plants as indicators of (paleo)ecology and (paleo)climate. Proc. Natl. Acad. Sci. U.S.A. 107, 19691–19695.

Korte, C., Hesselbo, S.P., Jenkyns, H.C., Rickaby, R.E.M., Spötl, C. 2009. Palaeoenvironmental significance of carbon- and oxygen-isotope stratigraphy of marine Triassic/Jurassic boundary sections in SW Britain. J. Geol. Soc., 166, 431-445

Korte, C., Hesselbo, S.P., 2011. Shallow-marine carbon- and oxygen-isotope and elemental records indicate icehouse-greenhouse cycles during the Early Jurassic. Paleoceanography, 26: PA4219.

Krassilov,V.A. 2003. Terrestrial palaeoecology and global change. Moscow, Pensoft

Krause, A.J., Mills, B.J.W., Zhang, S., Planavsky, N.J., Lenton, T.M., Poulton, S.W. 2018. Stepwise oxygenation of the Paleozoic atmosphere. Nat. Comm. 9, 4081

Kump, LR., 2018. Prolonged Late Permian early Triassic hyperthermal: failure of climate regulation? Phil.l Trans. Royal Soc. A, 376: 20170078; 10.1098/rsta.2017.0078

Kump L.R., Arthur M.A. 1999. Interpreting carbon-isotope excursions: Carbonates and organic matter. Chemical Geology 161, 181–198.

Kürschner, W.M. 1996. Leaf stomata as biosensors of palaeoatmospheric CO_2 levels. LPP Contributions Series 5, LPP Foundation, Utrecht.

Kürschner W.M. 2001. Leaf sensor for CO2 in deep time. Nature 411, 247–248.

Lindström, S., 2016. Palynofloral patterns of terrestrial ecosystem change during the end-Triassic event – a review. Geol. Mag. 153, 223-251.

Lindström, S., Van de Schootbrugge, B., Dybkjær, K., Pedersen, G.K., Fiebig,J., Nielsen, L.H., Richoz, S., 2012. No causal link between terrestrial ecosystem change and methane release during the end-Triassic mass extinction: Geology 40, 531–534, doi:10.1130/G32928.1.

Lindström, S., Pedersen, G.K., van de Schootbrugge, B., Hovedskov Hansen, K., Kuhlmann, N., Thein, J., Johansson, L., Petersen, H.I., Alwmark, C., Dybkjær, K., Weibel, R., Erlström, M., Nielsen, L.H., Oschmann, W., Tegner, C., 2015. Intense and widespread seismicity during the end-Triassic mass extinction due to emplacement of a large igneous province. Geology 43, 387–390.

Lindström, S., Van de Schootbrugge, B., Hansen, K. H., Pedersen G. K., Alsen, P., Thibault, N. , Dybkjær, K., Bjerrum C. J, Nielsen L.H. 2017. A new correlation of Triassic–Jurassic boundary successions in NW Europe, Nevada and Peru, and the Central Atlantic Magmatic Province: A time-line for the end-Triassic mass extinction. Palaeogeography, Palaeoclimatology, Palaeoecology 478, 80-102.

Liu, M., Sun, P., Them II, T.R, Li, Y., Sun, S., Gao, X., Huang, X., Tang, Y., 2020. Organic geochemistry of a lacustrine shale across the Toarcian Oceanic Anoxic Event (Early Jurassic) from NE China. Global and Planetary Change 191 (2020) 103214

López-Mondéjar, R., Brabcová, V., Štursová, M., Davidová, A., 1 Jansa, J., Cajthaml, T., Baldrian, P., 2018. Decomposer food web in a deciduous forest shows high share of generalist microorganisms and importance of microbial biomass recycling. The ISME Journal; https://doi.org/10.1038/s41396-018-0084-2

Marcinkiewicz, T., 1962. Rhaetian and Lias megaspores from borehole Mechowo near Kamień Pomorski and their stratigraphical value. Inst. Geol. Prace, 30, 469–493.

Marcinkiewicz, T., 1971. The stratigraphy of the Rhaetian and Lias in Poland based on megaspore investigations. Inst. Geol. Prace 65, 1–58.

McArthur, J. M., Algeo, T. J., van de Schootbrugge, B., Li, Q., Howarth, R. J., 2008. Basinal restriction, black shales, Re-Os dating, and the Early Toarcian (Jurassic) oceanic anoxic event. Paleoceanography, 23, PA4217, doi:10.1029/2008PA001607.

McElwain, J., Murphy, J. W., Hesselbo, S. P., 2005. Changes in carbon dioxide during an oceanic anoxic event linked to intrusion into Gondwana coals. Nature 435, 479-482.

Morgans, H.S., 1999. Lower and Middle Jurassic woods of the Cleveland basin (North Yorkshire) , England. Palaeontology 42, 303–328.

Mosbrugger, V. 1999. The nearest living relative method: In: Jones T.P. & Rowe N.P. (eds), Fossil plants and spores: modern techniques. 261–266, The Geol. Soc. London.

Pacyna, G. 2013. Critical review of research on the Lower Jurassic flora of Poland. Acta Palaeobot., 53, 141–163. DOI: 10.2478/acpa-2013-0015.

Pagani, M., Caldeira, K., Archer, D., Zachos, J.C., 2006. An ancient carbon mystery. Science 314, 1556-1557

Pálfy, J., Demeny, A., Haas, J., Hetényi, M., Orchard, M.J., Veto, I., 2001. Carbon isotope anomaly and other geochemical changes at the Triassic–Jurassic boundary from a marine section in Hungary. Geology 29, 1047–1050

Peti, L., Thibault, N., 2017. Abundance and size changes in the calcareous nannofossil Schizosphaerella – Relation to sea-level, the carbonate factory and palaeoenvironmental change from the Sinemurian to earliest Toarcian of the Paris Basin. Palaeogeogr., Palaeoclimatol., Palaeoecol., http://dx.doi.org/10.1016/j.palaeo.2017.06.019.

Philippe, M., Barbacka, M. Gradinaru, E., Iamandei, E., Iamandei , S., Kázmér, M., Popa, M., Szakmány, G., 2006. Fossil wood and Mid-Eastern Europe terrestrial palaeobiogeography during the Jurassic–Early Cretaceous interval. Rev. Palaeobot. Palynol. 142, 15–32

Pieńkowski, G., 2004, The epicontinental Lower Jurassic of Poland: Pol. Geol. Inst. Sp. Pap. 12, 1–154.

Pieńkowski, G., Waksmundzka, M., 2009. Palynofacies in Lower Jurassic epicontinental deposits of Poland: tool to interpret sedimentary environments. Episodes 32, 21–32

Pieńkowski, G., Niedźwiedzki, G., Waksmundzka, M., 2012. Sedimentological, palynological, and geochemical studies of the terrestrial Triassic–Jurassic boundary in northwestern Poland. Geol. Mag., 149, 308–332.

Pieńkowski, G., Niedźwiedzki, G., Brański, P., 2014. Climatic reversals related to the Central Atlantic magmatic province caused the end-Triassic biotic crisis—Evidence from continental strata in Poland, in Keller, G., and Kerr, A., eds., Volcanism, Impacts, and Mass Extinctions: Causes and Effects: Geol. Soc. Am. Sp. Paper 505, 263–286, doi:10.1130/2014.2505(13)

Pieńkowski, G. 2014. The first Early Jurassic ammonite find in central Poland. Vol. Jurassica 12, 99–104.

Pieńkowski, G., Schudack, M.E., Bosák, P., Enay, R., Feldman-Olszewska, A., Golonka, J., Gutowski, J., Herngreen, G.F.W., Jordan, P., Krobicki, M., Lathuiliere, B., Leinfelder, R.R., Michalík, J., Mönnig, E., Noe-Nygaard, N., Pálfy, J., Pint, A., Rasser, M.W., Reisdorf, A.G., Schmid, D.U., Schweigert, G., Surlyk, F., Wetzel, A., Wong, T.E. 2008. Jurassic. In: McCann, T. (ed) The Geology of Central Europe, Vol. 2: Mesozoic and Cenozoic. The Geol. Soc., 823–922.

Pieńkowski, G., Hodbod, M., Ullmann, C.V., 2016. Fungal decomposition of terrestrial organic matter accelerated Early Jurassic climate warming. Sci. Rep. 6. http://dx.doi.org/10.1038/srep31930

Poole, I., Kürschner, W.M. 1999. Stomatal density and index: the practice:. In: Jones T.P. & Rowe N.P. (eds), Fossil plants and spores: modern techniques, 257–261, The Geol. Soc. London.

Porter, S.J., Selby, D., Suzuki, K., Gröcke, D. 2013. Opening of a trans-Pangaean marine corridor during the Early Jurassic: Insights from osmium isotopes across the Sinemurian–Pliensbachian GSSP, Robin Hood's Bay, UK. Palaeogeogr., Palaeoclimatol., Palaeoecol. 375, 50–58

Porter, A. S., Yiotis, C., Montañez, I. P., McElwain, J. C., 2017. Evolutionary differences in δ13C detected between spore and seed bearing plants following exposure to a range of atmospheric O2:CO2 ratios; implications for paleoatmosphere reconstruction. Geochim. et Cosmochim. Acta 213, 517–533

Price, G.D., 1999. The evidence and implications of polar ice during the Mesozoic. Earth Sci. Rev. 48, 183–210.

Price, G., 2017. Stable isotope analyses of belemnite rostra from the Pliensbachian-Toarcian boundary: Implications for surface water conditions during deposition. International Meeting of Sedimentology, Toulouse, p. 724

Price, G.D., Baker, S.J., VanDeVelde, J., Clémence, M.E., 2016. High-resolution carbon cycle and seawater temperature evolution during the Early Jurassic (Sinemurian-Early Pliensbachian). Geochem., Geophys., Geosyst. 17, 3917–3928, doi:10.1002/2016GC006541

Rees, P. M. , Ziegler, A. M., and Valdes, P. J. 2000. Jurassic phytogeography and climates: new data and model comparisons. In: Huber, B. T.; Macleod, K. G.; and Wing, S. L., (eds): Warm climates in Earth history. Cambridge University Press, p. 297-318.

Reisdorf, A.G., Wetzel, A., Schlatter, R., Jordan, P., 2011. The Staffelegg Formation: a new stratigraphic scheme for the Early Jurassic of northern Switzerland. Swiss J. Geosci. 104, 97–146. DOI 10.1007/s00015-011-0057-1

Richardson, A. R., Eble, C. F., Hower, J. C. & O'Keefe, J. M. K. 2012. A critical re-examination of the petrology of the No. 5 Block coal in eastern Kentucky with special attention to the origin of inertinite macerals in the splint lithotypes. Int. J. Coal Geol. 98**,** 41–49

Riding , J.B., Leng, M.L., Kender, S., Hesselbo, S.P., Feist-Burkhardt, S. 2013. Isotopic and palynological evidence for a new Early Jurassic environmental perturbation. Palaeogeogr., Palaeoclimatol., Palaeoecol., 374, 16–27

Rodrigues, B., Silva, R.L., Reolid, M., Graciano, J., Filho, J.G.M., Duarte, L.V., 2019. Sedimentary organic matter and $\delta^{13}C_{Kerogen}$ variation on the southern Iberian palaeomargin (Betic Cordillera, SE Spain) during the latest Pliensbachian–Early Toarcian. Palaeogeogr. Palaeoclimatol., Palaeoecol. 534, https://doi.org/10.1016/j.palaeo.2019.109342

Royer, D.L., Scott, L.W., Beerling, D.J., Jolley, D.W., Koch, P.L., Hickey L.J., Berner, R.A. 2001. Palaeobotanical evidence for near present day levels of atmospheric CO_2 during part of the Tertiary. Science 292, 2310–2313.

Ruebsam, W., Mayer, B., Schwark, L. 2019. Cryospheric carbon dynamics control early Toarcian global warming and sea level evolution. Glob. Planet. Chang. 172, 440-453

Ruebsam, W., Al-Husseini, M. 2020. Calibrating the Early Toarcian (Early Jurassic) with stratigraphic black holes (SBH). Gondwana Res. 82, 317–336

Ruebsam, W., Reolid, M., Schwark, L., 2020. δ13C of terrestrial vegetation records Toarcian CO2 and climate gradients. Sci. Rep. 10:117 | https://doi.org/10.1038/s41598-019-56710-6 1

Ruhl, M., Deenen, M.H.L., Abels, H.A., Bonis, N.R., Krijgsman, W., Kürschner, W.M., 2010. Astronomical constraints on the duration of the Early Jurassic Hettangian stage and recovery rates following the end-Triassic mass extinction (St Audrie's Bay/East Quantoxhead, UK). Earth Planet. Sci. Lett. 295, 262–276.

Ruhl, M., Kürschner, W.M., 2011, Multiple phases of carbon cycle disturbance from large igneous province formation at the Triassic-Jurassic transition: Geology 39, 431–434, doi:10.1130/G31680.1.

Ruhl, M., Hesselbo, S.P., Hinnov, L., Jenkyns, H.C., Xu, W., Storm, M.S., Riding, J.B., Minisini, D., Ullmann, C.V., Leng, M.J., 2016. Astronomical constraints on the duration of the Early Jurassic Pliensbachian Stage and global climatic fluctuations. Earth Planet. Sci. Lett. 455, 149–165.

Schöllhorn, I., Adatte, T., Van de Schootbrugge, B., Houbenc, A., Charbonniera, G., Janssenc, N., Föllmi, K. 2020. Climate and environmental response to the break-up of Pangea during the Early Jurassic (Hettangian-Pliensbachian); the Dorset coast (UK) revisited. Glob. Planet. Chang. https://doi.org/10.1016/j.gloplacha.2019.103096

Schouten, S., Van Kaam-Peters, H.M.E., Rijpstra, W.I.C., Schoell, M., Sinninghe Damsté, J.S., *2000.* Effects of an oceanic anoxic event on the stable carbon isotopic composition of early Toarcian carbon. Am. J. Sci. 300, 1-22

Schubert, B. A., Jahren, A. H., 2012. The effect of atmospheric CO2 concentration on carbon isotope fractionation in C3 land plants. Geochim. Cosmochim. Acta 96, 29–43

Slater, S.M, Twitchett, R.J., Danise, S., Vajda, V. 2019. Substantial vegetation response to Early Jurassic global warming with impacts on oceanic anoxia. Nat. Geosci., https://doi.org/10.1038/s41561-019-0349-z

Steinthorsdottir, M., Jeram, A.J., McElwain, J.C., 2011. Extremely elevated CO_2 at the Triassic–Jurassic boundary. Palaeogeogr., Palaeoclimatol., Palaeoecol. 308, 418–432.

Steinthorsdottir, M., Vajda V. 2015. Early Jurassic (late Pliensbachian) CO_2 concentrations based on stomatal analysis of fossil conifer leaves from eastern Australia. Gondwana Res. 27, 932–939.

Storm, M.S., Hesselbo, S.P., Jenkyns, H.C., Ruhl, M., Ullmann, C. V., Xu, W., Leng, M.J., Riding, J.B., Gorbanenko, O., 2020. Orbital pacing and secular evolution of the Early Jurassic carbon cycle. Proc. Nat. Acad. Sci. U.S.A 117, 3974-3982. doi: 10.1073/pnas.1912094117

Suan, G., Mattioli, E., Pittet, B., Mailliot, S., Lécuyer, C., 2008. Evidence for major environmental perturbation prior to and during the Toarcian (Early Jurassic) oceanic anoxic event from the Lusitanian Basin, Portugal. Paleoceanography 23, PA1202. http://dx.doi.org/10.1029/2007PA001459.

Suan, G., Mattioli, E., Pittet, B., Lécuyer, C., Suchéras-Marx, B., Duarte, L.V., Philippe, M., Reggiani, L., Martineau, F., 2010. Secular environmental precursors to Early Toarcian (Jurassic) extreme climate changes. Earth Planet. Sci. Lett. 290, 448-458

Suan, G., Van de Schootbrugge, B., Adatte, T., Fiebig, J., Oschmann, W., 2015. Calibrating the magnitude of the Toarcian carbon cycle perturbation. Paleoceanography 30, 495–509, doi:10.1002/2014PA002758.

Them, T. R. III, Gill, B.C., Caruthers A.H., Gröcke, D.R., Tulsky E.T., Martindale, R.C., Poulton, T.P., Smith, P.L., 2017a. High-resolution carbon isotope records of the Toarcian Oceanic Anoxic Event (Early Jurassic) from North America and implications for the global drivers of the Toarcian carbon cycle. Earth Planet. Sci. Lett. 459, 118–126

Them T.R. III, Gill, B.C., Selby, D., Gröcke, D.R., Friedman, R.M., Owens, J.D.,2017b. Evidence for rapid weathering response to climatic warming during the Toarcian Oceanic Anoxic Event. Sci. Rep. 7:5003.

Thibault, N., Ruhl, M., Ullmann, C. V., Korte, C., Kemp, D.B., Gröcke, D.R., Hesselbo, S.P., 2017. The wider context of the Lower Jurassic Toarcian oceanic anoxic event in Yorkshire coastal outcrops, UK. Proc. Geol. Ass. 129, 372-391.

Thierry, J., Barrier, E. et al. (39 co-authors), 2000. Map 8. Middle Toarcian (180–178 Ma). In: Dercourt, J., Gaetani, M., Vrielynck, B., Barrier, E., Biju-Duval, B., Brunet, M.-F., Cadet, J.P., Crasquin, S., Sandulescu, M. (Eds.), Atlas Peri-Tethys Paleogeographical Maps, vol. I-XX.CCGM/CGMW, Paris, map 8.

Ullmann, C.V., R. Boyle, R., Duarte, L.V., S. P. Hesselbo, S.P., Kasemann, S.A., Klein, T., Lenton, T.M., V. Piazza, V., Aberhan, M. 2020. Warm afterglow from the Toarcian Oceanic Anoxic Event drives the success of deep-adapted brachiopods. Sci. Rep. 10*:* 6549 https://doi.org/10.1038/s41598-020-63487-6

Vandenbroucke, M., Largeau, C., 2007. Kerogen origin, evolution and structure. Org. Geochem. 38, 719–833

Van de Schootbrugge, B., J. L. Payne, A. Tomasovych, J. Pross, J. Fiebig, M. Benbrahim, K. B. Föllmi, and T. M. Quan, 2008. Carbon cycle perturbation and stabilization in the wake of the Triassic-Jurassic boundary mass-extinction event. Geochem. Geophys. Geosyst. 9, Q04028, doi:10.1029/2007GC001914.

Van de Schootbrugge, B., Bachan, A., Suan, G., Richoz, S., Payne, J. L., 2013. Microbes, mud and methane: Cause and consequence of recurrent Early Jurassic anoxia following the end-Triassic mass extinction. Palaeontology, 56, 685–709.

Van de Schootbrugge, B., Little, C. T. S., Püttmann, W., Guex, J., Fraguas, A., Wonik, T., Blau, T., Pross,J., van der Weijst, C. M. H., Wignall, P. B., Luppold, F. W., Oschmann, W., Hunze, S., Richoz, S., Herrle, J. O., Meister, C., Fiebig, J. and Suan, G.**,** 2019. The Schandelah Scientific Drilling Project: A 25-million year record of Early Jurassic palaeo- environmental change from northern Germany. Newsletters on Stratigraphy, 52, 249–296.

Whiteside, J. H., Olsen, P. E., Eglinton, T., Brookfield, M. E., Sambrotto, R. N. 2010. Compound-specific carbon isotopes from Earth's largest flood basalt eruptions directly linked to the end-Triassic mass extinction. Proc. Natl. Acad. Sci. U.S.A. 107, 6721–6725.

Woodland, A.W. (ed.), 1971. The Llanbedr (Mochras Farm) Borehole. Rep. No. 71/18, Inst. Geol. Sci., London, 115 pp.

Woodward, F.I. 1987. Stomatal numbers are sensitive to increases in CO2 from pre-industrial levels. Nature 327, 617–618.

Wong, K., Mason, E., Brune, S., East, M, Edmonds, M. Zahirovic, S., 2019. Deep Carbon Cycling Over the Past 200 Million Years: A Review of Fluxes in Different Tectonic Settings. Front. Earth Sci. 7, 263. Doi: 10.3389/feart.2019.00263

Wolf, A. A., Drake B. G., Erickson, J. E., Megonigal, J. P.,2007. An oxygen-mediated positive feedback between elevated carbon dioxide and soil organic matter decomposition in a simulated anaerobic wetland. Glob. Chang. Biol. 13, 2036–2044, 10.1111/j.1365-2486.2007.01407.x

Wotzlaw, J.F., Guex, J., Bartolini, A., Gallet, Y., Krystyn, L., McRoberts, C.A, Taylor, D., Schoene, B., Schaltegger, U., 2014. Towards accurate numerical calibration of the Late Triassic: High-precision U-Pb geochronology constraints on the duration of the Rhaetian. Geology, doi:10.1130/G35612.1

Xie, S., Sun, B., Yan, D., Xiao, L., Wei, L. 2006. Leaf cuticular characters of Ginkgo and implications for palaeoatmospheric CO2 in the Jurassic. Progr. Nat. Sci. 16, 258–263.

Xu, W., Ruhl, M., Jenkyns H.C., Hesselbo, S. P., Riding, J.B., Selby, D., Naafs, B.D.A., Weijers, J.W.H., Pancost, R.D., Tegelaar, E.W., Idiz, E.F., 2017. Carbon sequestration in an expanded lake system during the Toarcian oceanic anoxic event. Nat. Geosci. 10, 129–134

Xu, W., Ruhl, M., Jenkyns H.C, Leng, M.L., Huggett, J.M., Minisini, D., Ullmann, C.V., Riding, J.B., Weijers, J.W.H., Storm, M. S., Percival, L.M.E., Tosca, N.J., Idiz, E.F., I., Tegelaar, E.W., Hesselbo, S.P. 2018. Evolution of the Toarcian (Early Jurassic) carbon cycle and global climatic controls on local sedimentary processes (Cardigan Bay Basin, UK). Earth Planet. Sci. Lett. 484, 396–411.

Zhou, Z. 2009. An overview of fossil Ginkgoales. Palaeoworld 18, 1–22. DOI: 10.1016/j.palwor.2009.01.001

Figure captions

Fig. 1. A - Paleogeographical map of Europe in Early Jurassic showing positions of Kaszewy and Mochras boreholes (after Thierry et al. (2000); B – Polish Lower Jurassic basin with location of Kaszewy borehole: 1 – inferred maximum range of the Lower Jurassic deposits, 2 – maximum thickness of the Lower Jurassic deposits – 500 and 1000 m isopachs (after Pieńkowski 2004).

Fig. 2. Stratigraphic correlation between Kaszewy ($\delta^{13}C_{wood}$ - black) and Mochras borehole (blue – $\delta^{13}C_{TOC}$, dashed red – $\delta^{13}C_{carbonate}$ and black dots - $\delta^{13}C_{wood}$), using carbon isotope chemostratigraphy, sequence stratigraphy and biostratigraphical proxies. Reference C isotope curves of the profile Mochras (biostratigraphically calibrated) are based on Storm et al. 2020 ($\delta^{13}C_{TOC}$, $\delta^{13}C_{wood}$)and Katz et al.2005 ($\delta^{13}C_{carbonate}$). For the Rhaetian section, the reference curve is based on Ruhl et al. (2010) (black). TOC content in Kaszewy is shown – marine (blue line) and continental (red line). Note two options of chemostratigraphic correlation of the upper Sinemurian – lower Pliensbachian transition. The first option (green bars) implies condensation and incomplete $\delta^{13}C_{wood}$ dataset in Kaszewy in the lowermost Pliensbachian, while the second correlation (pink bars) implies strong erosion at the sequence boundaries V and VI, resulting in absence of most of the lower Pliensbachian and atypical (for Polish basin) sedimentary development of both upper Sinemurian and lower Pliensbachian. Considering the above reasons, $\delta^{13}C_{wood}$ correlation and correlations with other profiles (Fig. 3), the first option was adopted as more likely, despite more similar general isotope trends when adopting the second option.

Fig. 3. Chemostratigraphic correlation of Kaszewy profile with other C isotope curves and major negative CIEs observed in reference sections and recognized in Kaszewy (see Supplementary data 3). All curves are based on $\delta^{13}C_{organic}$, except for Basque-Cantabrian Basin (Quesada et al, 2005) where

the $\delta^{13}C$ values are based on belemnites. The Toarcian Oceanic Anoxic Event (= Jenkyns Event) section is presented in detail in Fig. 4.

Fig. 4. Chemostratigraphic correlation of the lower Toarcian section and the Toarcian Oceanic Anoxic Event (= Jenkyns Event) of Kaszewy profile with selected C isotope curves, showing correlation of C isotope steps T. 1-5 (defined in other profiles in the Polish basin - Hesselbo and Pieńkowski 2011) with other C isotope curves and composite picture of T-OAE. Biostratigraphy: *P.sp. – Pleuroceras spinatum* zone (Pliensbachian), *D.Tenuicostaum – Dactylioceras tenuicostatum* zone (Toarcian), *H.falciferum – Harpoceras falciferum* zone (Toarcian). Note that positions of *Dactylioceras* tenuicostatum/ *Harpoceras f*alciferum boundary (sub-Boreal realm) and the *Dactylioceras polymorphum*/*Harpoceras levisoni* boundary (Mediterranean Realm) may slightly differ (Ruebsam and Al-Husseini 2020). $\delta^{13}C_{org}$ trends: r.l. – rising limb, pl. – plateau, vl – valley, f.l. – falling limb; A-O - $\delta^{13}C_{org}$ steps (after Ruebsam and Al-Husseini 2020). Kaszewy profile is much more expanded than coeval marine sections, while most of the section corresponds to the falling limb of T-OAE (5 steps – T. 1-5) and rising limb is less complete, likely with condensations or hiatuses in the upper part (see Hesselbo and Pieńkowski 2011).

Fig. 5. Plot of $\delta^{13}C_{wood}$/ TOC_{cont} showing statistically significant positive correlation (Pearson) between the two variables in 224 samples, both for linear (lin) and exponential (exp) fit: r = 0.59 for exponential fit; r = 0.53 for linear fit. The p-value is <0.00001. The result is statistically significant at p<.05. For the Rhaetian (66 samples) r = 0.16; for the Lower Jurassic (159 samples) r = 0.57; Spearman's Rank Correlation Coefficient (in 224 samples): Rs = 0.61, p val = 6.44^{-24}; the result is significant the significance threshold 0.001 (see Supplementary 4). The correlation is interpreted as a result of differentiated decomposition of terrestrial organic matter related to climate changes, but also other factors could have influenced the observed relationship.

Fig. 6. Four photographs from the lower Toarcian samples, showing wood strongly decomposed by fungi and fungal mycelia and spores: A – sample 1235.6 m: fungal mycelia; B – sample 1201.1 m: fungal mycelia and spores; C – sample 1201.1 m: fungal mycelia and spores; D – sample 1246.9 m: segmented fungal mycelia; E – sample 1201.1 m: fungal spore. Scale for A-E = 20 µ.

Fig. 7. Inferred temperature trends in Rhaetian and Early Jurassic in the Kaszewy profile based on stomatal index and macrofloral data and tentatively on the $\delta^{13}C_{wood}$/ TOC_{cont} plot (Fig. 5) . Macroflora represents three general assemblages: *Czekanowskia-Pseudotorellia* (relatively drier-cooler conditions), *Baiera-Ginkgoites-Sphenobaiera* (relatively warmer and more humid) and *Neocalamites-Schizoneura* (humid). Climatic trends are indicated with their inferred stratigraphic age.

Supplementary data

Supplementary data 1: Kaszewy borehole, carbon isotope and TOC values

Supplementary data 2: Van Krevelen plot, Kaszewy borehole

Supplementary data 3: Chemostratigraphic correlation of major carbon isotope excursions

Supplementary data 4: Spearman's Rank Correlation Coefficient calculation (in 224 samples)

The authors declare no conflict of interest

*Significant relationship between $\delta^{13}C_{wood}$ and TOC_{cont} in the studied Rhaetian to Lower Jurassic strata

*Efficiency of terrestrial biodegradation is pCO_2 and temperature specific at northern mid palaeolatitudes

* $\delta^{13}C_{wood}$, TOC_{cont} and temperature respond to carbon cycle forcing

*Stomatal index results are compatible with the interpreted temperature trends

*Reliable $\delta^{13}C$ chemostratigraphic correlation of marine and marginal/non-marine deposits demonstrated

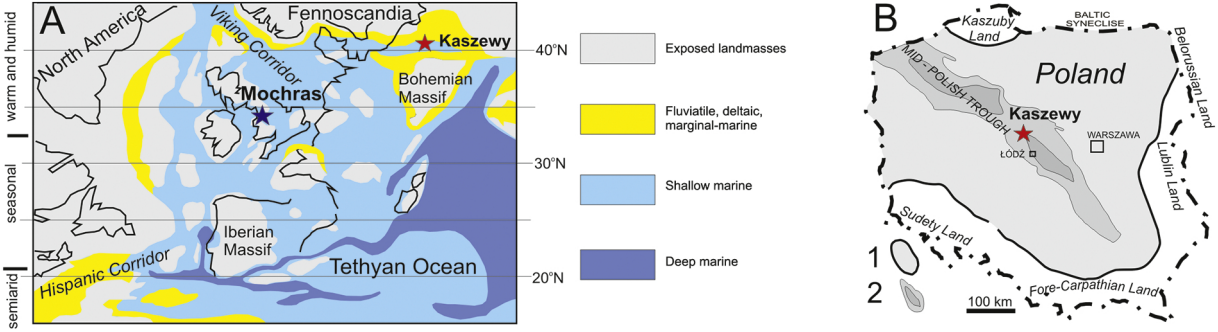
A
North America
Fennoscandia
Viking Corridor
Kaszewy
Bohemian Massif
Mochras
Iberian Massif
Hispanic Corridor
Tethyan Ocean
warm and humid
seasonal
semiarid
40°N
30°N
20°N
Exposed landmasses
Fluviatile, deltaic, marginal-marine
Shallow marine
Deep marine
B
Kaszuby Land
BALTIC SYNECLISE
Poland
MID - POLISH TROUGH
Kaszewy
WARSZAWA
ŁÓDŹ
Belorussian Land
Lublin Land
Sudety Land
Fore-Carpathian Land
1
2
100 km

Figure 1

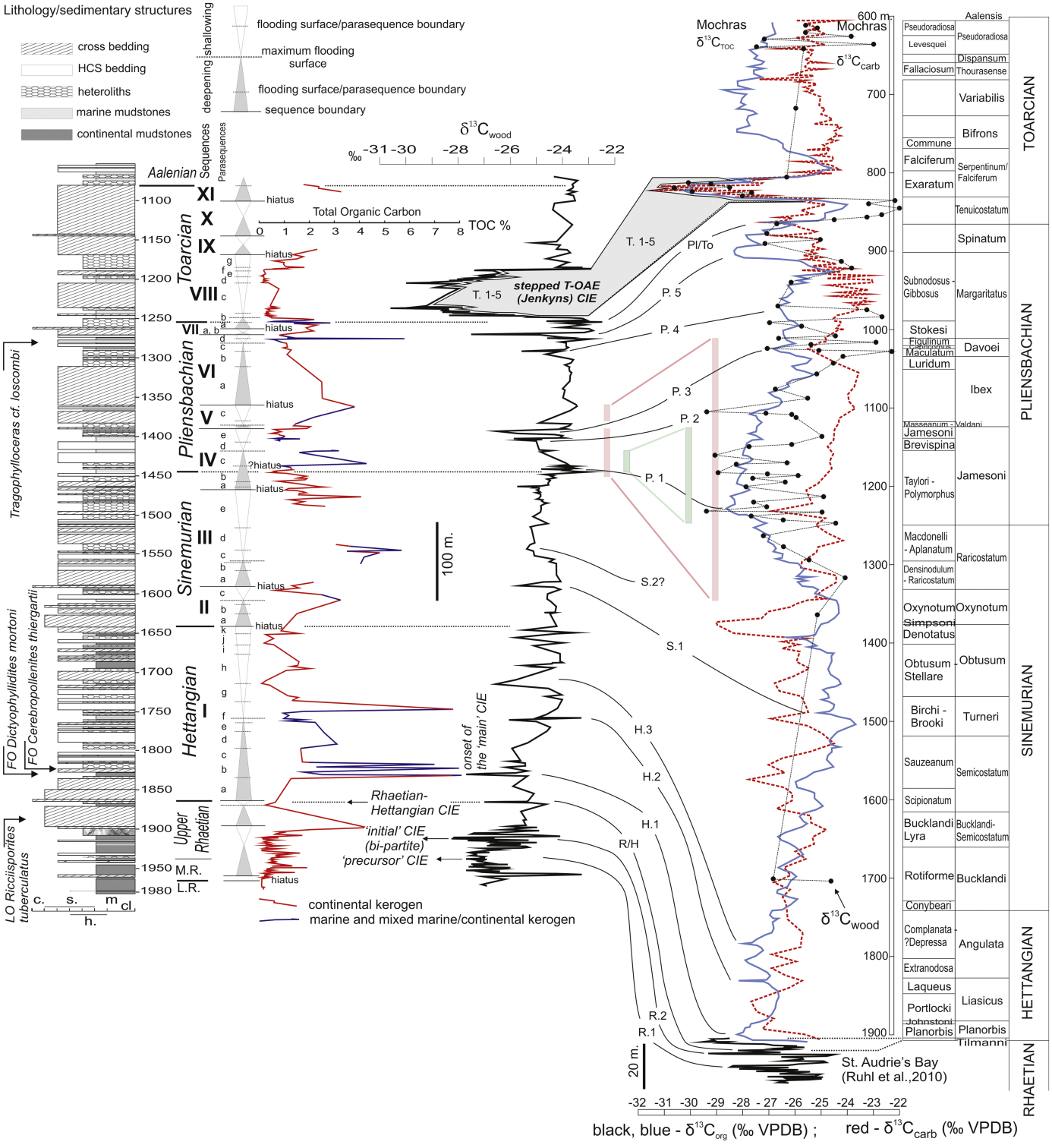
Lithology/sedimentary structures
cross bedding
HCS bedding
heteroliths
marine mudstones
continental mudstones
shallowing
deepening
flooding surface/parasequence boundary
maximum flooding surface
flooding surface/parasequence boundary
sequence boundary
Sequences
Parasequences
Aalenian
Toarcian
Pliensbachian
Sinemurian
Hettangian
Upper Rhaetian
XI
X
IX
VIII
VII
VI
V
IV
III
II
I
hiatus
?hiatus
Total Organic Carbon
TOC %
δ13Cwood
‰ -31 -30 -28 -26 -24 -22
T. 1-5
Pl/To
P. 5
P. 4
P. 3
P. 2
P. 1
stepped T-OAE (Jenkyns) CIE
S.2?
S.1
H.3
H.2
H.1
R/H
R.2
R.1
100 m.
20 m.
onset of the 'main' CIE
Rhaetian-Hettangian CIE
'initial' CIE (bi-partite)
'precursor' CIE
Tragophylloceras cf. loscombi
FO Dictyophyllidites mortoni
FO Cerebropollenites thiergartii
LO Ricciisporites tuberculatus
M.R.
L.R.
c. s. m cl
h.
Mochras
Mochras δ13CTOC
δ13Ccarb
δ13Cwood
600 m
700
800
900
1000
1100
1200
1300
1400
1500
1600
1700
1800
1900
Aalensis
Pseudoradiosa
Levesquei
Fallaciosum
Dispansum
Thouarsense
Variabilis
Bifrons
Commune
Falciferum
Exaratum
Serpentinum/ Falciferum
Tenuicostatum
Spinatum
Subnodosus - Gibbosus
Margaritatus
Stokesi
Figulinum
Maculatum
Davoei
Luridum
Ibex
Masseanum - Valdani
Jamesoni
Brevispina
Taylori - Polymorphus
Jamesoni
Macdonelli - Aplanatum
Densinodulum - Raricostatum
Raricostatum
Oxynotum
Simpsoni
Denotatus
Obtusum Stellare
Obtusum
Birchi - Brooki
Turneri
Sauzeanum
Scipionatum
Semicostatum
Bucklandi Lyra
Bucklandi-Semicostatum
Rotiforme
Bucklandi
Conybeari
Complanata - ?Depressa
Extranodosa
Angulata
Laqueus
Portlocki
Johnstoni
Liasicus
Planorbis
Tilmanni
Planorbis
TOARCIAN
PLIENSBACHIAN
SINEMURIAN
HETTANGIAN
RHAETIAN
St. Audrie's Bay (Ruhl et al.,2010)
-32 -31 -30 -29 -28 -27 -26 -25 -24 -23 -22
continental kerogen
marine and mixed marine/continental kerogen
black, blue - δ13Corg (‰ VPDB) ;
red - δ13Ccarb (‰ VPDB)

Figure 2

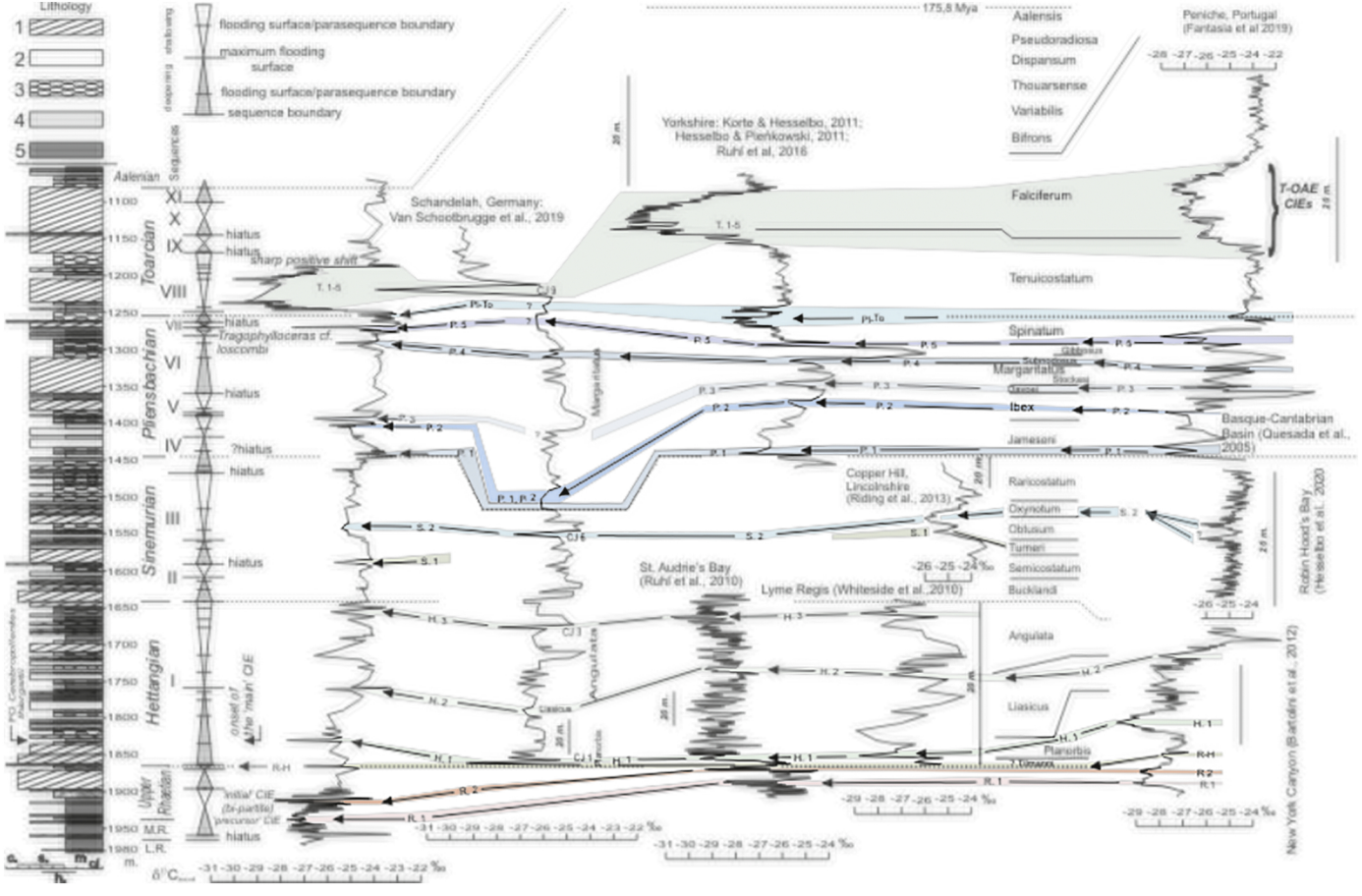
Lithology
1
2
3
4
5
flooding surface/parasequence boundary
maximum flooding surface
flooding surface/parasequence boundary
sequence boundary
Sequences
Aalenian
Toarcian
Pliensbachian
Sinemurian
Hettangian
Upper Rhaetian
M.R.
L.R.
m.
hiatus
sharp positive shift
Tragophylloceras cf. loscombi
onset of the 'main' CIE
'initial' CIE (bi-partite) 'precursor' CIE
Schandelah, Germany: Van Schootbrugge et al., 2019
Yorkshire: Korte & Hesselbo, 2011; Hesselbo & Pieńkowski, 2011; Ruhl et al, 2016
175,8 Mya
Aalensis
Pseudoradiosa
Dispansum
Thouarsense
Variabilis
Bifrons
Falciferum
Tenuicostatum
Spinatum
Margaritatus
Ibex
Jamesoni
Raricostatum
Oxynotum
Obtusum
Turneri
Semicostatum
Bucklandi
Angulata
Liasicus
Planorbis
Penhe, Portugal (Fantasia et al 2019)
T-OAE CIEs
Basque-Cantabrian Basin (Quesada et al., 2005)
Copper Hill, Lincolnshire (Riding et al., 2013)
St. Audrie's Bay (Ruhl et al., 2010)
Lyme Regis (Whiteside et al., 2010)
Robin Hood's Bay (Hesselbo et al., 2020)
New York Canyon (Bartolini et al., 2012)
$\delta^{13}C_{carb}$ ‰

Figure 3

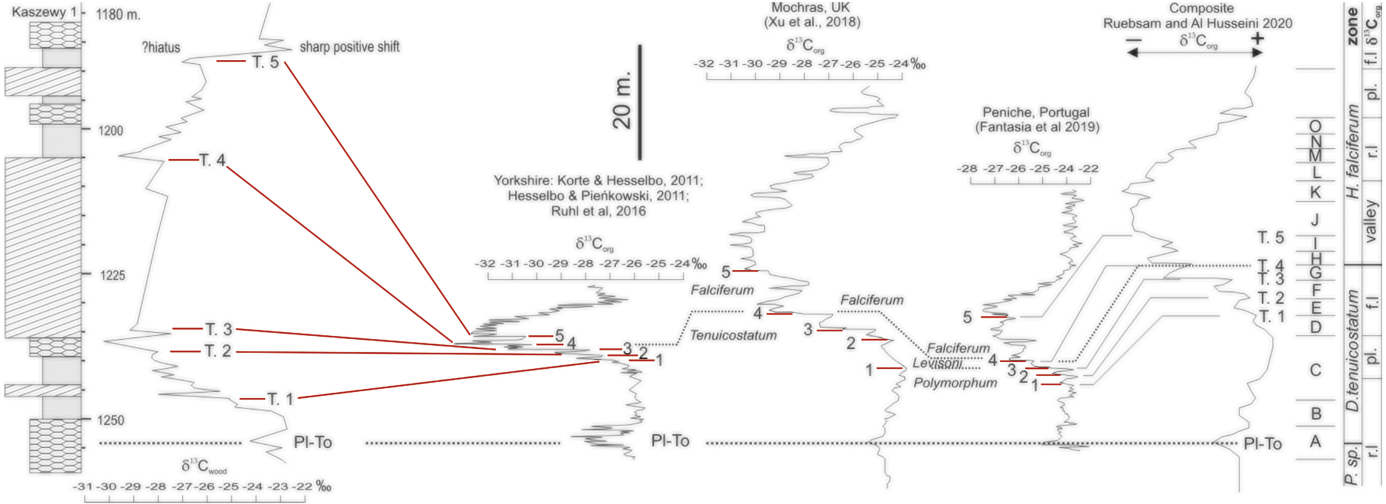
Kaszewy 1
1180 m.
1200
1225
1250
?hiatus
sharp positive shift
T. 5
T. 4
T. 3
T. 2
T. 1
Pl-To
δ13Cwood
-31 -30 -29 -28 -27 -26 -25 -24 -23 -22 ‰
20 m.
Yorkshire: Korte & Hesselbo, 2011;
Hesselbo & Pieńkowski, 2011;
Ruhl et al, 2016
δ13Corg
-32 -31 -30 -29 -28 -27 -26 -25 -24 ‰
Falciferum
Tenuicostatum
Mochras, UK
(Xu et al., 2018)
δ13Corg
-32 -31 -30 -29 -28 -27 -26 -25 -24 ‰
Falciferum
Levisoni
Polymorphum
Peniche, Portugal
(Fantasia et al 2019)
δ13Corg
-28 -27 -26 -25 -24 -22
Composite
Ruebsam and Al Husseini 2020
δ13Corg
zone
δ13Corg
f.l
pl.
r.l
H. falciferum
O
N
M
L
K
J
I
H
G
F
E
D
C
B
A
valley
D. tenuicostatum
P. sp.

Figure 4

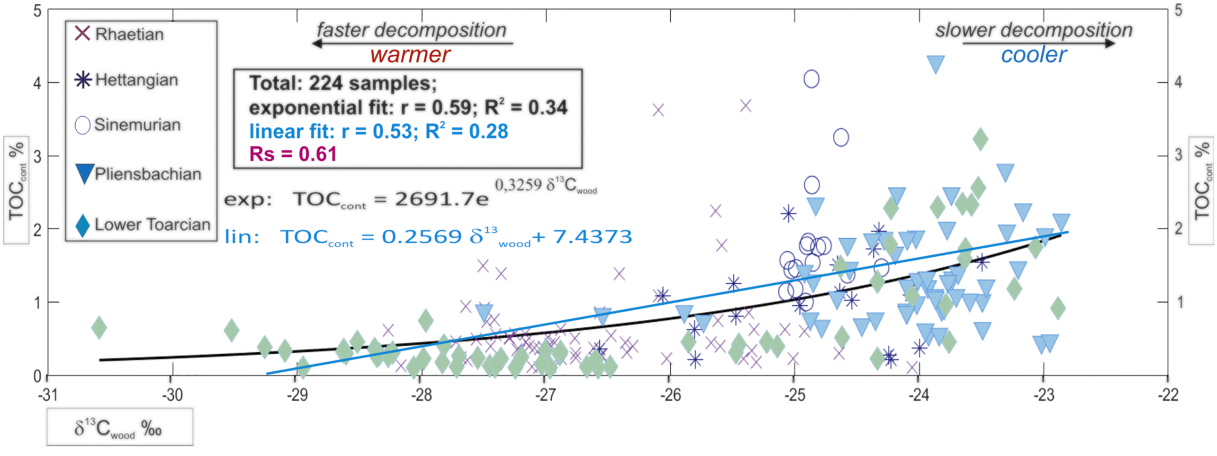
Rhaetian
Hettangian
Sinemurian
Pliensbachian
Lower Toarcian
faster decomposition
warmer
slower decomposition
cooler
Total: 224 samples;
exponential fit: r = 0.59; R² = 0.34
linear fit: r = 0.53; R² = 0.28
Rs = 0.61
exp: TOC_cont = 2691.7e^(0,3259 δ13C_wood)
lin: TOC_cont = 0.2569 δ13C_wood + 7.4373
TOC_cont %
δ13C_wood ‰
5
4
3
2
1
0
-31
-30
-29
-28
-27
-26
-25
-24
-23
-22

Figure 5

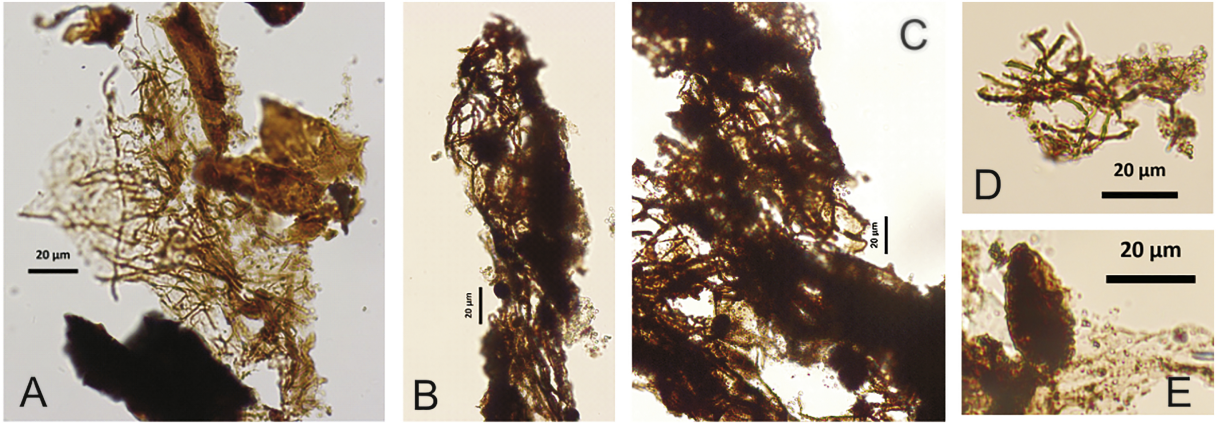

Figure 6

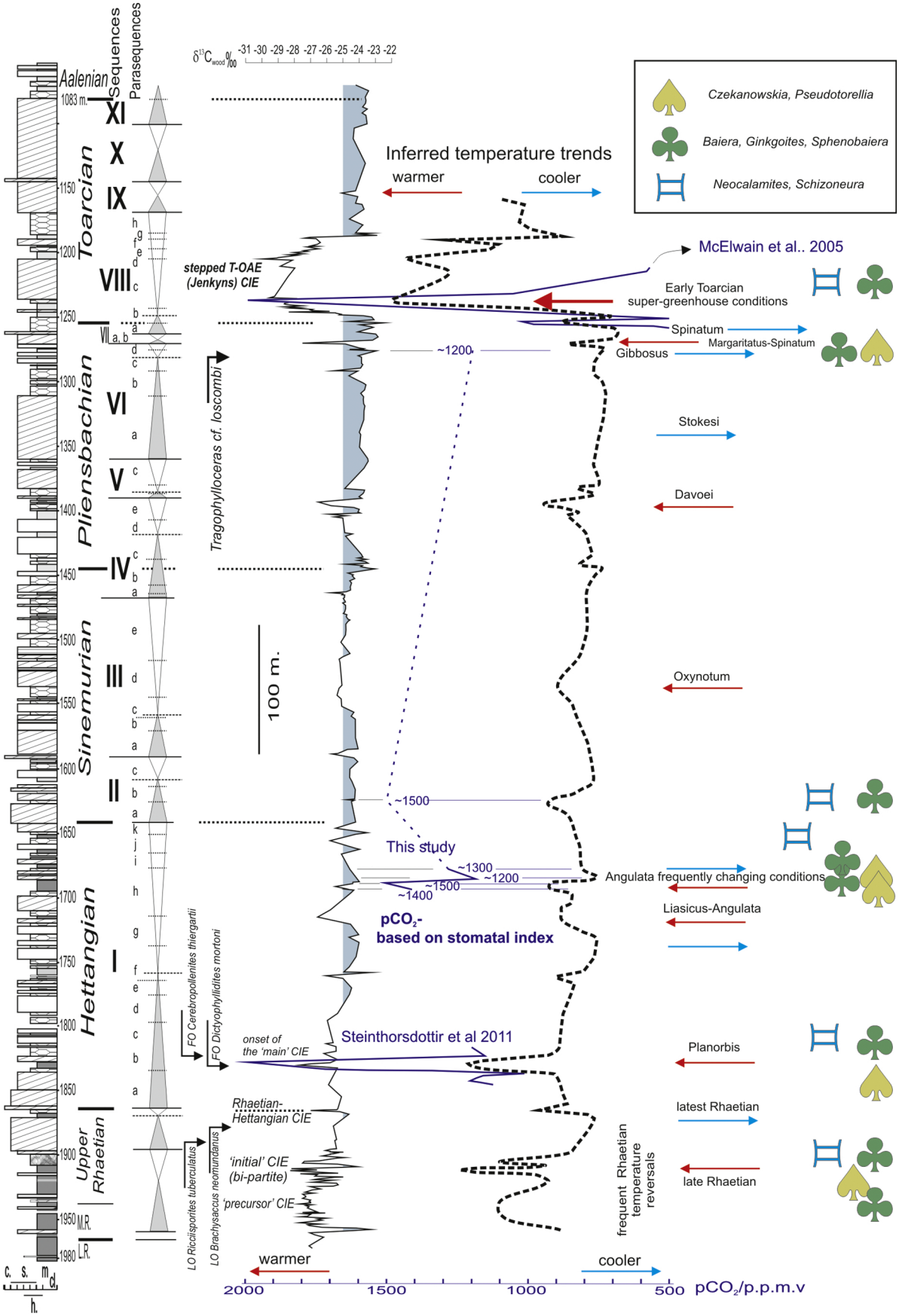
Sequences
Parasequences
Aalenian
1083 m.
Toarcian
Pliensbachian
Sinemurian
Hettangian
Upper Rhaetian
M.R.
L.R.
δ13Cwood ‰
-31 -30 -29 -28 -27 -26 -25 -24 -23 -22
Inferred temperature trends
warmer
cooler
Czekanowskia, Pseudotorellia
Baiera, Ginkgoites, Sphenobaiera
Neocalamites, Schizoneura
McElwain et al.. 2005
stepped T-OAE (Jenkyns) CIE
Early Toarcian super-greenhouse conditions
Spinatum
Margaritatus-Spinatum
Gibbosus
Tragophylloceras cf. loscombi
~1200
Stokesi
Davoei
100 m.
Oxynotum
~1500
This study
~1300
~1200
~1500
~1400
Angulata frequently changing conditions
Liasicus-Angulata
pCO2- based on stomatal index
FO Cerebropollenites thiergartii
FO Dictyophyllidites mortoni
onset of the 'main' CIE
Steinthorsdottir et al 2011
Planorbis
Rhaetian-Hettangian CIE
latest Rhaetian
'initial' CIE (bi-partite)
'precursor' CIE
frequent Rhaetian temperature reversals
late Rhaetian
LO Ricciisporites tuberculatus
LO Brachysaccus neomundanus
warmer
cooler
2000
1500
1000
500
pCO2/p.p.m.v

Figure 7